Major influence of a 'smoke and mirrors' effect caused by wave reflection on early diastolic coronary arterial wave intensity

Jonathan P. Mynard[1,2,3] (iD), Daniel J. Penny[1,2,3,4] and Joseph J. Smolich[1,2,4]

[1] *Heart Research, Clinical Sciences, Murdoch Children's Research Institute, Parkville, VIC 3052, Australia*
[2] *Department of Paediatrics, University of Melbourne, Parkville, VIC 3052, Australia*
[3] *Department of Cardiology, Royal Children's Hospital, Parkville, VIC 3052, Australia*
[4] *Institute of Reproduction and Development, Monash University, Clayton, VIC, Australia*

Edited by: Don Bers & Michael Shattock

Key points

- Coronary wave intensity analysis (WIA) is an emerging technique for assessing upstream and downstream influences on myocardial perfusion.
- It is thought that a dominant backward decompression wave (BDW_{dia}) is generated by a distal suction effect, while early-diastolic forward decompression (FDW_{dia}) and compression (FCW_{dia}) waves originate in the aorta.
- We show that wave reflection also makes a substantial contribution to FDW_{dia}, FCW_{dia} and BDW_{dia}, as quantified by a novel method. In 18 sheep, wave reflection accounted for ~70% of BDW_{dia}, whereas distal suction dominated in a computer model representing a hypertensive human.
- Non-linear addition/subtraction of mechanistically distinct waves (e.g. wave reflection and distal suction) obfuscates the true contribution of upstream and downstream forces on measured waves (the 'smoke and mirrors' effect).
- The mechanisms underlying coronary WIA are more complex than previously thought and the impact of wave reflection should be considered when interpreting clinical and experimental data.

Abstract Coronary arterial wave intensity analysis (WIA) is thought to provide clear insight into upstream and downstream forces on coronary flow, with a large early-diastolic surge in coronary flow accompanied by a prominent backward decompression wave (BDW_{dia}), as well as a forward decompression wave (FDW_{dia}) and forward compression wave (FCW_{dia}). The BDW_{dia} is believed to arise from distal suction due to release of extravascular compression by relaxing myocardium, while FDW_{dia} and FCW_{dia} are thought to be transmitted from the aorta into the coronary arteries. Based on an established multi-scale computational model and high-fidelity measurements from the proximal circumflex artery (Cx) of 18 anaesthetized sheep, we present evidence that wave reflection has a major impact on each of these three waves, with a non-linear addition/subtraction of reflected waves obscuring the true influence of upstream and downstream forces through concealment and exaggeration, i.e. a 'smoke and mirrors' effect. We also describe methods, requiring additional measurement of aortic WIA, for unravelling the separate influences of wave reflection *versus* active upstream/downstream forces on coronary waves. Distal wave reflection accounted for ~70% of the BDW_{dia} in sheep, but had a lesser influence (~25%) in the computer model representing a hypertensive human. Negative reflection of the BDW_{dia} at the coronary–aortic junction attenuated the Cx FDW_{dia} (by ~40% in sheep) and augmented Cx FCW_{dia} (~5-fold), relative to the corresponding aortic waves. We conclude that wave reflection

---

has a major influence on early-diastolic WIA, and thus needs to be considered when interpreting coronary WIA profiles.

Introduction

Wave intensity analysis (WIA) has been used to study the upstream and downstream forces contributing to the distinctive pattern of coronary arterial blood flow (Sun *et al.* 2000, 2004; Davies *et al.* 2006*a*; Hadjiloizou *et al.* 2008; Smolich & Mynard, 2016), with 'waves' (i.e. incremental changes in blood pressure and velocity) arising from active forces such as myocardial contraction/relaxation or from wave reflection. Given the diastolic dominance of coronary arterial flow, there has been particular interest in the wave dynamics underlying the early-diastolic flow surge and how waves around this time are affected by various forms of heart disease and medical intervention (Davies *et al.* 2006*a*, 2011; Kyriacou *et al.* 2012; Lockie *et al.* 2012; De Silva *et al.* 2013; Claridge *et al.* 2015). Three main waves have been consistently identified during this early-diastolic phase of the cardiac cycle (Fig. 1). [In this paper 'early-diastole' refers to the period soon after the left ventricle starts to relax, and hence encompasses the short period before aortic valve closure, sometimes referred to as protodiastole.] A flow-increasing backward decompression wave (BDW_{dia}) is believed to arise from the release of extravascular compressive forces on intramyocardial vessels, producing a suction effect that propagates back towards the coronary ostium (Davies *et al.* 2006*a*). In addition, two forward waves, a flow-decreasing forward decompression wave (FDW_{dia}) and a flow-increasing forward compression wave (FCW_{dia}), are thought to arise from transmission of corresponding aortic waves into the coronary arteries; these aortic waves are generated by the early diastolic fall in left ventricular (LV) cavity pressure and the pressure/flow 'rebound' caused by aortic valve closure respectively (Davies *et al.* 2006*a*).

While the current explanations for early-diastolic coronary arterial waves are intuitive, they have not been confirmed by any direct approach, while close inspection of published coronary WIA data suggest that the picture is not yet complete. Specifically, although correlations have been observed between BDW_{dia} magnitude and indices of isovolumic relaxation derived from LV cavity pressure, the reported R^2 values (0.21–0.35) suggest that more than 60% of the variability in BDW_{dia} magnitude is currently unexplained (Kyriacou *et al.* 2012; Ladwiniec *et al.* 2016). Indeed, it is unclear why the BDW_{dia} is much larger than a backward compression wave occurring during iso-

volumic contraction (BCW_{ic}, Fig. 1), despite published data suggesting that the rate of change of intramyocardial pressure rise (leading to BCW_{ic}) and fall (leading to BDW_{dia}) are comparable (Heineman & Grayson, 1985; Stein *et al.* 1985; Rabbany *et al.* 1989). In addition, although it is generally assumed that the FDW_{dia} and FCW_{dia} are simply transmitted from the aorta into the coronary arteries (Davies *et al.* 2006*a*), several published figures suggest that the FDW_{dia} and FCW_{dia} may be less and more prominent, respectively, in the coronary arteries than aorta (Hughes *et al.* 2008; Lu *et al.* 2012), with the basis of such differences yet to be defined.

A potentially significant but largely unexplored factor that may influence the early-diastolic coronary waves is wave reflection, with backward waves reflecting proximally at the coronary ostium and forward waves reflecting distally in the coronary arterial network. Due to the large impedance mismatch between the coronary arteries and aorta (Davies *et al.* 2006*a*), the BCW_{ic} is considered to undergo near-complete negative reflection at the coronary ostium, leading to a subsequent forward decompression wave (FDW_{ic}, Fig. 1); however, it is unclear whether the BDW_{dia} also undergoes such reflection and what effect this might have on the FCW_{dia} and FDW_{dia}. In addition, partial reflection of the early-systolic forward compression wave (FCW_{sys}) in the coronary arterial bed leads to a second backward compression wave (BCW_{sys}), but it is unclear whether the FDW_{dia} is similarly reflected, and whether the resulting reflected decompression wave might contribute to the BDW_{dia}.

The foregoing phenomena have particular relevance due to the possibility that a measured wave intensity peak (herein referred to as a 'wave') may arise from a combination of factors, such as the simultaneous influence of an active force *and* wave reflection. Intuitively, the combination of two mechanistically distinct waves would be expected to have an additive effect if both waves are compression waves or both are decompression waves, or a cancelling effect if compression and decompression waves combine. However, the specific nature of such additive or cancelling effects, and a method for unravelling the separate contributions of an active force and wave reflection to a composite wave, have yet to be defined.

The aim of this study was to investigate the extent to which each of the three main early diastolic coronary waves, currently presumed to simply arise from upstream (FDW_{dia} and FCW_{dia}) and downstream (BDW_{dia}) active

forces (Davies *et al.* 2006*a*), are also influenced by wave reflection. We first demonstrate that there is a *non-linear* additive or cancelling effect on wave intensity when two mechanisms contribute to a measured wave. Using a previously described multi-scale computational model of the coronary circulation (Mynard *et al.* 2014; Mynard & Smolich, 2016*a*), we show that wave reflection effects lead to concealment of the coronary FDW_{dia} and augmentation of the BDW_{dia} and FCW_{dia}, which we term a 'smoke and mirrors' effect. We also describe methods for unravelling the contributions of active forces and wave reflection underlying measured coronary waves. These principles and methods were initially tested with the computational model and then examined in an experimental model where simultaneous aortic and coronary WIA were obtained under baseline conditions and following an increase in arterial blood pressure, with or without coronary vasoconstriction.

Methods

Ethical approval

Experimental studies (described towards the end of this section) were approved by the Monash University Animal Ethics Committee and conformed to the guidelines of the National Health and Medical Research Council of Australia.

Wave intensity

Wave intensity is defined as the product of incremental changes in pressure and velocity ($dPdU$) (Parker & Jones, 1990). Since this quantity is sample time-dependent, a time-corrected wave intensity is often used, calculated as $WI = (dP/dt)(dU/dt)$ (Ramsey & Sugawara, 1997; Penny *et al.* 2008). The forward component (WI_+) and backward component (WI_-) of wave intensity are calculated via $WI_\pm = \pm(dP/dt \pm \rho c\, dU/dt)^2/(4\rho c)$, with forward waves having positive WI and backward waves having negative WI. Cumulative wave intensity (CI), related to the energy of a wave (Davies *et al.* 2006*a*; Mynard & Smolich, 2016*b*), is defined as the integral of $WI_\pm$ over the duration of a given wave. Waves that have a pressure-increasing effect are called 'compression waves', whereas waves that have a pressure-decreasing effect are called 'decompression waves' (sometimes also referred to as 'suction' or 'expansion' waves). The four possible wave types are forward compression (FCW), forward decompression (FDW), backward compression (BCW) and backward decompression (BDW) waves.

Non-linear addition and subtraction of coronary waves

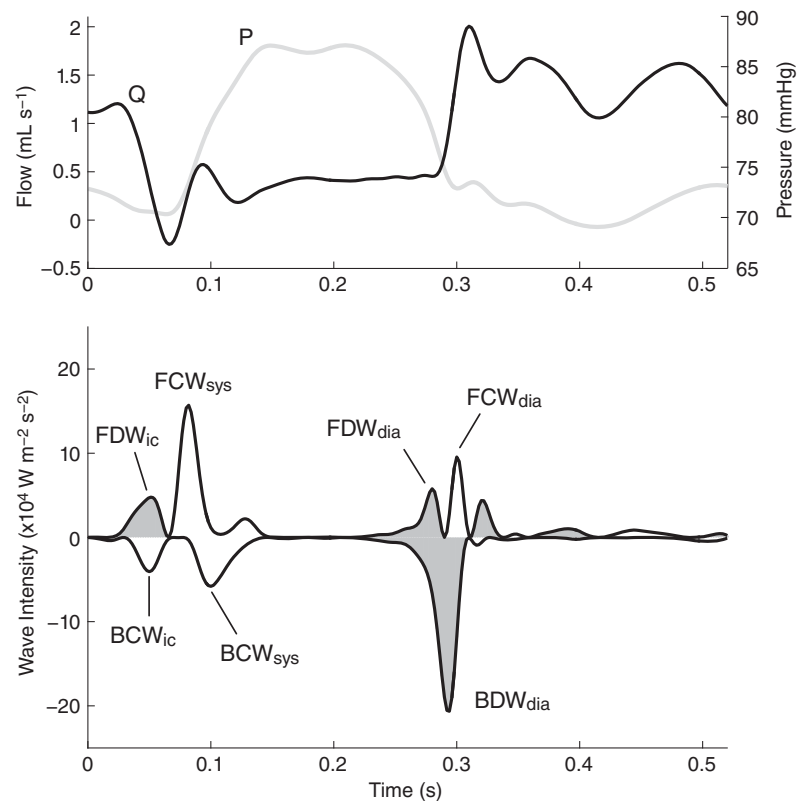Since coronary arterial waves may arise from an active mechanism (e.g. a distal suction effect arising in the

Figure 1. Circumflex coronary pressure (P), flow (Q) and wave intensity from an adult sheep
The major waves, which are also present in humans, are labelled according to wave type (FCW, FDW, BCW, BDW; forward/backward compression/decompression wave) and phase of the cardiac cycle (ic, isovolumic contraction; sys, early-systole; dia, early-diastole). Decompression (i.e. pressure-decreasing) waves are shaded.

intramyocardial vessels) and also from wave reflection, it is possible that both phenomena could simultaneously influence the wave intensity profile. In this section, we show that the addition or subtraction of two mechanistically distinct waves is non-linear (i.e. $1 + 1 \neq 2$). For simplicity of notation, in this section we use the non-time-corrected form of wave intensity, but the same principles also apply to the time-corrected form.

Consider the situation where two waves propagate in the same direction, but one arises via passive reflection of some incident wave ($\mathrm{d}P\mathrm{d}U_{\text{reflected}}$) and the other is generated from an active process such as a change in extravascular pressure due to myocardial relaxation ($\mathrm{d}P\mathrm{d}U_{\text{active}}$). If these two mechanistically distinct waves affect pressure and velocity at the same time, the total change in pressure will be $\mathrm{d}P_{\text{reflected}} + \mathrm{d}P_{\text{active}}$ and the total change in velocity will be $\mathrm{d}U_{\text{reflected}} + \mathrm{d}U_{\text{active}}$. The wave intensity of the resulting combined wave is therefore

$$\mathrm{d}P\mathrm{d}U_{\text{combined}} = (\mathrm{d}P_{\text{reflected}} + \mathrm{d}P_{\text{active}}) \, (\mathrm{d}U_{\text{reflected}} + \mathrm{d}U_{\text{active}}) \quad (1)$$

Importantly, we see that these waves do not add linearly, that is

$$\mathrm{d}P\mathrm{d}U_{\text{combined}} \neq \mathrm{d}P\mathrm{d}U_{\text{reflected}} + \mathrm{d}P\mathrm{d}U_{\text{active}} \quad (2)$$

For example, consider two backward decompression waves (BDW_1 and BDW_2) for which $\mathrm{d}P$ and $\mathrm{d}U$ have numerical values of -5 and 5 respectively for both waves, with BDW_1 arising from wave reflection and BDW_2 arising from myocardial relaxation (Fig. 2A). Wave intensity of each wave in isolation would be -25 ($\mathrm{d}P\mathrm{d}U = -5 \times 5$). However, if these two waves occur at the same time, the resulting combined BDW will not have an amplitude of -50, but rather $\mathrm{d}P\mathrm{d}U_{\text{combined}} = (-5 - 5) \times (5 + 5) = -100$. This

illustrates the principle that when two compression waves or two decompression waves combine, the resultant wave is much larger than the sum of the contributing waves in isolation.

Now consider what happens if two waves with opposing pressure effects combine. For example, if an FDW with wave intensity $\mathrm{d}P\mathrm{d}U = -5 \times -6 = 30$ combines with an FCW with wave intensity $\mathrm{d}P\mathrm{d}U = 4 \times 5 = 20$, the resulting combined wave does not have an amplitude of $20 + 30 = 50$, nor is it $30 - 20 = 10$; rather it is $\mathrm{d}P\mathrm{d}U_{\text{combined}} = (4 - 5) \times (5 - 6) = 1$ (Fig. 2B). Thus, there is a non-linear cancelling effect when a compression wave combines with a decompression wave.

Coronary reflection and myocardial contraction/relaxation

With these principles of wave addition and subtraction in mind, we therefore tested two main hypotheses:

Hypothesis 1 (Fig. 3A): The measured early-diastolic coronary BDW ($\mathrm{BDW}_{\text{dia}}$) arises from a combination of two distinct processes, (i) an active suction effect caused by a rapid fall in vascular external compression due to myocardial relaxation (mr), which in isolation would cause a backward decompression wave designated BDW_{mr}; and (ii) passive distal reflection of the early diastolic FDW transmitted from the aorta into the coronary arteries ($\mathrm{FDW}_{\text{A}\rightarrow\text{C}}$), which in isolation would cause a wave designated $\mathrm{BDW}_{\text{ref}}$. The BDW_{mr} and $\mathrm{BDW}_{\text{ref}}$ add non-linearly to produce the $\mathrm{BDW}_{\text{dia}}$, which is thus substantially larger than the sum of the intensities of the individual waves. This hypothesis is illustrated in Fig. 3A.

Hypothesis 2 (Fig. 3B): The coronary $\mathrm{BDW}_{\text{dia}}$ undergoes almost complete negative reflection when it reaches the coronary ostium due to the much lower impedance of the aorta compared with the coronary artery. The resulting
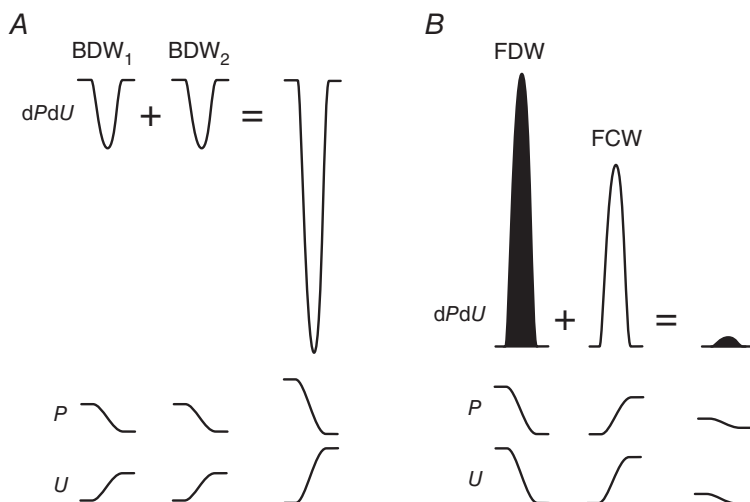

Figure 2. Illustration of non-linear wave addition and subtraction
A, when two backward decompression waves (BDW_1 and BDW_2) combine, the wave intensity ($\mathrm{d}P\mathrm{d}U$) of the resultant single combined wave is greater than the sum of the $\mathrm{d}P\mathrm{d}U$ of the two waves in isolation. *B*, when a forward decompression wave (FDW) combines with a forward compression wave (FCW), there is a non-linear cancelling effect. The non-linear nature of wave intensity addition and subtraction may be understood by assessing the underlying pressure (*P*) and velocity (*U*) changes associated with the waves.

reflected FCW (FCW_{ref}) has a non-linear cancelling effect on the aortic FDW transmitted into the coronary arteries ($FDW_{A \to C}$), with the resultant measured coronary wave (FDW_{dia}) being relatively small compared with aortic FDW_{dia}. In addition, the FCW_{ref} has a non-linear additive effect on the FCW related to valve closure that is transmitted from the aorta into the coronary arteries ($FDW_{A \to C}$), with the resultant combined coronary wave (FDW_{dia}) being relatively large compared with aortic FDW_{dia}. This hypothesis is illustrated in Fig. 3B.

Distinguishing wave reflection and upstream/downstream forces

Based on the above principles, we propose that the coronary $FDW_{A \to C}$, i.e. the coronary FDW_{dia} that would occur in the absence of BDW_{dia} reflection, may be estimated by assuming that the aortic FCW_{sys} and FDW_{dia} are identically transmitted into the coronary artery, and hence the following ratios (known as transmission coefficients) should also be approximately equal:

$$\frac{\text{Coronary FDW}_{A \to C}}{\text{Aortic FDW}_{dia}} \approx \frac{\text{Coronary FCW}_{sys}}{\text{Aortic FCW}_{sys}} \quad (3)$$
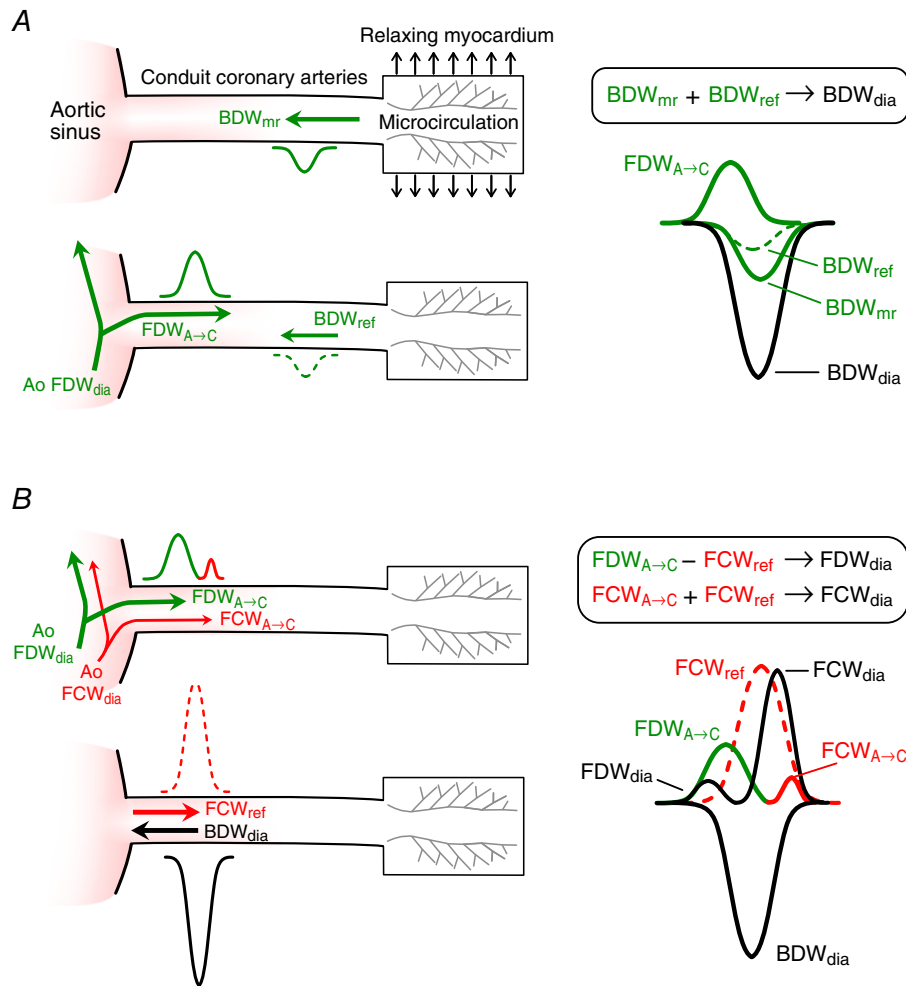

Figure 3. Illustration of the mechanisms underlying early diastolic coronary waves
A, the measured BDW_{dia} arises in part from a distal suction effect caused by myocardial relaxation (BDW_{mr}); a second contribution to BDW_{dia} arises from distal reflection (BDW_{ref}) of the aortic forward decompression wave (Ao FDW_{dia}) that passes into the coronary arteries ($FDW_{A \to C}$). The BDW_{mr} and BDW_{ref} add non-linearly to produce a prominent BDW_{dia}. *B*, the BDW_{dia} undergoes near-complete negative reflection at the coronary ostium, where it encounters a large drop in characteristic impedance. This produces a reflected forward compression wave (FCW_{ref}) that non-linearly subtracts from the $FDW_{A \to C}$ and augments the valve closure-related forward compression wave ($FCW_{A \to C}$) that originates in the aorta (Ao FCW_{dia}), leading to the measured early-diastolic forward waves (FDW_{dia} and FCW_{dia}). Measured waves are indicated in black while component compression and decompression waves are indicated in red and green respectively (colour in online version only). Waves arising from reflection are indicated with dashed lines. [Colour figure can be viewed at wileyonlinelibrary.com]

This may be rearranged to estimate the coronary $FDW_{A \rightarrow C}$, which is the only unknown:

$$\text{Coronary } FDW_{A \rightarrow C} \approx \text{Coronary } FCW_{sys}$$
$$\times \left(\frac{\text{Aortic } FDW_{dia}}{\text{Aortic } FCW_{sys}} \right) \quad (4)$$

In the same way, the coronary $FCW_{A \rightarrow C}$ may also be estimated as

$$\text{Coronary } FCW_{A \rightarrow C} \approx \text{Coronary } FCW_{sys}$$
$$\times \left(\frac{\text{Aortic } FCW_{dia}}{\text{Aortic } FCW_{sys}} \right) \quad (5)$$

If we calculate an early systolic coronary reflection index as BCW_{sys}/FCW_{sys} and assume that the same degree of wave reflection occurs during early diastole (this assumption will be examined in the Results section using the computational model), then the BDW_{ref} can be estimated from $FDW_{A \rightarrow C}$ via

$$\text{Coronary } BDW_{ref} \approx \text{Coronary } FDW_{A \rightarrow C}$$
$$\times \left(\frac{\text{Coronary } BCW_{sys}}{\text{Coronary } FCW_{sys}} \right) \quad (6)$$

Equations (4) to (6) can be applied to peak wave intensity, cumulative intensity (wave area) or incremental changes in pressure and velocity ($dP_{\pm}$ and $dU_{\pm}$). The coronary BDW_{mr} intensity can then be estimated by (i) calculating dP_{-} and dU_{-} associated with BDW_{ref}, via eqn (6), (ii) calculating dP_{-} and dU_{-} associated with BDW_{mr}, by subtracting values for BDW_{ref} from values for BDW_{dia}, and (iii) calculating BDW_{mr} wave intensity as the product of the resulting BDW_{mr} dP_{-} and dU_{-} values. This may be expressed as

$$\text{Coronary } BDW_{mr} = dP_{mr-}dU_{mr-} = (dP_{dia-} - dP_{ref-})$$
$$\times (dU_{dia-} - dU_{ref-}) \quad (7)$$

In this equation, dP and dU may be replaced by dP_{-}/dt and dU_{-}/dt for calculation of time-corrected BDW_{mr}. The contribution of BDW_{mr} to the measured BDW_{dia} may then be quantified as

$$BDW_{mr} \text{ contribution} = \frac{BDW_{mr}}{BDW_{mr} + BDW_{ref}} \quad (8)$$

and expressed as a percentage, noting that this is not the same as BDW_{mr}/BDW_{dia} due to the non-linear addition effects described above. Note that eqn (7), and hence also eqn (8), depend on instantaneous values of dP and dU and can therefore only be used in relation to peak intensity. This means that the cumulative intensity of the BDW_{ref} but not the BDW_{mr} can be estimated.

Model description

The model used in this study is based on our previous work (Mynard *et al.* 2012, 2014; Mynard & Smolich, 2016*a*). Aside from some input parameters discussed below, all aspects of the model have been described in these previous papers and we therefore provide only a brief summary below. Model parameters are provided in the Appendix.

First, a one-dimensional (1D) model of the major right dominant conduit coronary arterial system was derived from measurements obtained in humans by Dodge *et al.* (1992) (Fig. 4*A*). The standard non-linear 1D equations in these networks were solved as in Mynard & Nithiarasu (2008), making use of a physiologically realistic non-linear elastic pressure–area relationship (Mynard *et al.* 2012) and the approximate velocity profile method of Bessems *et al.* (2007) to estimate the viscous friction term.

Second, the coronary model was placed within a closed-loop model of the cardiovascular system (Mynard *et al.* 2012) that included the four heart chambers and valves, lumped systemic and pulmonary vascular beds, and single 1D segments approximating each of the major vascular networks (Fig. 4*B*); a similar model but with anatomically based vascular networks was described by Mynard and Smolich (2015), but this level of detail is not required for the present study.

Third, the coronary microcirculation was represented by a lumped parameter model (Fig. 4*C*), instances of which were inserted at all distal outlets of the 1D conduit artery model (boxes in Fig. 4*A*). This microvascular model, based on studies by Bruinsma *et al.* (1988) and Spaan *et al.* (2000), was divided into subepicardial, midwall and subendocardial layers. Each layer consisted of two compartments, whose volumes were governed by the compliances C_1 and C_2, approximately corresponding to small arteries and veins respectively in the layer. Each layer also contained three volume-dependent resistances, R_1 and R_2, which were modulated by the volume in compartments 1 and 2 respectively, and a middle resistance (R_m) modulated by the volume in both compartments. Compartment volume depended on the difference between intravascular pressure and intramyocardial pressure (p_{im}). As in Mynard *et al.* (2014), we assumed that p_{im} arises from (i) cavity-induced extracellular pressure (CEP), i.e. transmission of ventricular cavity pressure into the ventricular wall, and (ii) shortening-induced intracellular pressure (SIP), arising from the thickening of shortening myofibrils that leads to compression of adjacent blood vessels (Heineman & Grayson, 1985; Rabbany *et al.* 1989; Algranati *et al.* 2010). For a full description of the model, including equations, see Mynard *et al.* (2014).

Parameters for the cardiovascular model are provided in the Appendix and were chosen to represent an older

adult with stage I hypertension, typical of patients encountered in clinical studies of coronary wave intensity (Davies *et al.* 2006*a*; Hadjiloizou *et al.* 2008; Narayan *et al.* 2015), with aortic pressures of 155/84 mmHg, cardiac output 4.9 L min^{-1}, systemic vascular resistance 1.8 mmHg.s mL^{-1} and aortic wave speed 9.0 m s^{-1} (Mitchell *et al.* 2003). Distributed arterial wave reflection was approximated by introducing linear tapering in the single equivalent systemic artery. Coronary resistance was adjusted using an iterative algorithm (Mynard *et al.* 2014; Mynard & Smolich, 2016*a*) to achieve a total coronary flow equal to 4.5% of cardiac output; due to the higher

perfusion pressure, a 52–90% increase in intramyocardial resistance was required compared with the original model, depending on the region and transmural layer. Note that the model was not intended to represent the sheep studied in the experimental model; rather, it was used to investigate wave dynamics in a system approximately representative of patients encountered clinically.

Model-based analysis of coronary wave mechanisms

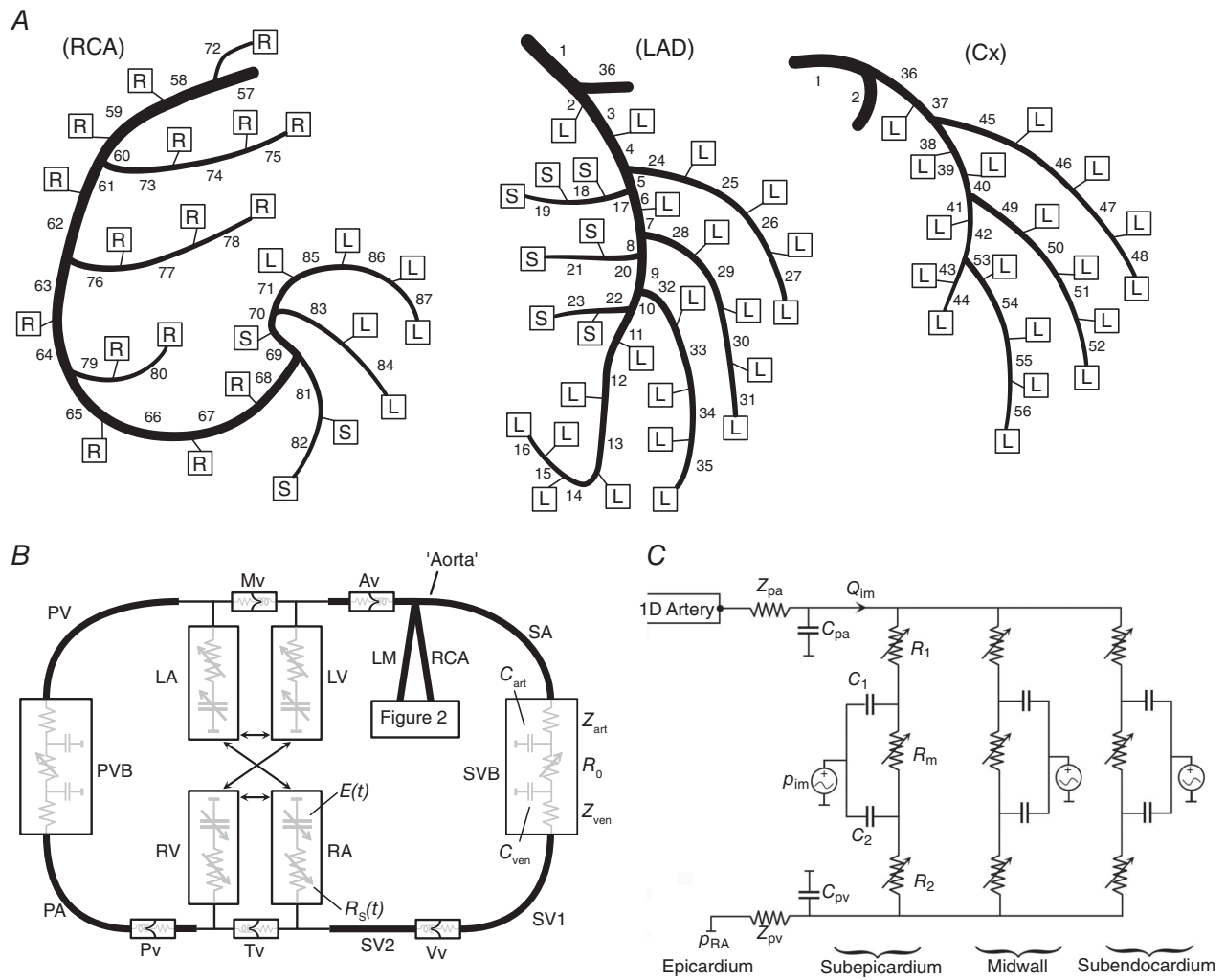With the reference simulation of coronary haemo-dynamics established, we sought to elucidate the

Figure 4. Schematics of the model components
A, one-dimensional (1D) model of the conduit coronary arteries; *B*, closed-loop cardiovascular model within which the coronary model resides; *C*, the coronary microcirculation model. Boxes in *A* indicate attachment of terminal 1D segments to instances of the lumped parameter microcirculatory model shown in *C*, which supply parts of the right ventricular free wall ('R' boxes), left ventricular free wall ('L' boxes) or septum ('S' boxes). Full details of the right dominant coronary network shown in *A* are provided in Mynard & Smolich (2016*a*). Note that the proximal end of the SA segment is referred to as the aorta. Abbreviations: Av, aortic valve; Cx, circumflex coronary artery; LA, left atrium; LM, left main coronary artery; LV, left ventricle; Mv, mitral valve; PA, pulmonary artery; Pv, pulmonary valve; PV, pulmonary vein; PVB, pulmonary vascular bed; RA, right atrium; RCA, right coronary artery; RV, right ventricle; SA, systemic artery; SVB, systemic vascular bed; SV, systemic vein; Tv, tricuspid valve; Vv, venous valve.

mechanisms underlying observed waves with two 'virtual experiments'.

First, to identify waves generated from within the myocardium, aortic waves were prevented from passing into the coronary arteries by enforcing a reflection coefficient of −1 at the coronary ostia, achieved by prescribing a constant end-diastolic pressure at the boundary; this maintained the same reflection conditions for backward-running coronary waves. To ensure this did not cause any indirect changes to the intramyocardial pump effect, we also prescribed the same time-varying intramyocardial pressures and resistances as in the reference case.

Second, to elucidate the interactions between waves transmitted from the aorta into the coronary arteries and those originating in the coronary microcirculation, we took the aortic pressure waveform from the reference case and prescribed this at the coronary inlets after applying a phase shift (i.e. time delay) that varied between −110 ms and +110 ms in 10-ms steps (a total of 23 simulations). This meant that all aortic waves passing into the coronary arteries were variably delayed whereas waves arising from intramyocardial pump effects in the microcirculation were fixed, allowing clear identification of the origin of different waves and the effects of wave addition and subtraction.

We also tested the assumption that the coronary reflection index is similar during early systole and early diastole. Starting with the reference simulation, this was done by (i) removing the intramyocardial pressure source (p_{im} in Fig. 4C) to ensure backward waves arose only via reflection and (ii) retaining the p_{im}-related changes in coronary resistance from the reference simulation, noting that changes in resistance are likely to be a key factor determining the instantaneous reflection index. Then, the reflection index (BCW_{sys}/FCW_{sys}) at different times in the cardiac cycle was assessed in the proximal left anterior descending artery (LAD) by introducing delays in the incoming aortic waves. Distal reflection indexes during early systole (BCW_{sys}/FCW_{sys}) and early diastole (BDW_{dia}/FDW_{dia}) were also assessed in all terminal 1D vessels (no delays applied).

Unless otherwise stated, results are presented for the proximal LAD, since this is frequently the subject of clinical investigation, but similar findings were also obtained in other vessels, including the circumflex artery. A sensitivity analysis was performed to evaluate to what extent the contribution of wave reflection *versus* myocardial relaxation on BDW_{dia} depends on aortic mean and pulse pressures (adjusted via systemic vascular bed resistance and aortic wave speed respectively), intramyocardial resistance (parallel combination of R_1 from all layers, see Fig. 4C) or compliance (C_1 and C_{pa}), monitoring location along the entire length of the LAD or coronary wave speed.

Experimental preparation

The experimental preparation was similar to that described previously (Penny *et al.* 2008). Eighteen Border-Leicester cross ewes weighing 49.6 ± 4.8 kg (mean ± SD) were anaesthetized with an intramuscular injection of ketamine (5 mg kg^{-1}) and xylazine (0.1 mg kg^{-1}) followed by intravenous α-chloralose (25–50 mg kg^{-1}). Anaesthesia was maintained with intravenous α-chloralose infused at a rate of 12–25 mg kg h^{-1}. After intubation of the trachea, animals were ventilated with a large animal respirator (model 607; Harvard Apparatus, Dover, MA, USA) with ventilation adjusted to maintain arterial O$_2$ tension at 100–120 mmHg and arterial CO$_2$ tension at 35–40 mmHg. Body temperature was maintained at 39–40°C with a heating pad and towel covering.

The neck was incised in the midline, and polyvinyl catheters were advanced through the left external jugular vein to the superior vena cava for fluid and drug infusion. A 5-Fr. micromanometer-tipped catheter (MPC-500; Millar Instruments, Houston, TX, USA) was inserted into the left common carotid artery, and its tip was advanced into the ascending aorta, just above the leaflets of the aortic valve, to measure high-fidelity blood pressure. After exposure of the heart and central vessels through a left thoracotomy performed in the fourth intercostal space and incision of the pericardium over the pulmonary trunk and left atrium, cannulae were inserted through purse string sutures in the aortic arch and left atrial appendage, and connected to fluid-filled polyvinyl tubing. Transit time flow probes (Transonics Systems, Ithaca, NY, USA) were placed around the ascending aorta (20 or 24 mm) and proximal circumflex coronary artery (2 or 4 mm). A second MPC-500 catheter was inserted through the roof of the left atrium and passed across the mitral valve into the LV cavity.

Experimental protocol

Aortic blood pressure measured via the fluid-filled catheter was referenced to atmospheric pressure at the level of the mid-thoracic vertebral spines and calibrated against a manometer before each experiment. Aortic and LV micromanometers were connected to transducer control units (TCB-500; Millar Instruments), while ascending aortic and coronary flow probes were interfaced with a flowmeter (model T206; Transonic Systems). Animals underwent one of two interventions: (i) in 11 animals, aortic blood pressure and coronary vascular resistance were increased by inhibition of NO synthesis via intravenous infusion of the stereospecific NO synthase inhibitor N^{ω}-nitro-L-arginine (L-NNA, 25 mg kg^{-1}) over 10 min (Penny & Smolich, 2002); (ii) in seven animals, mean central aortic blood pressure was raised to a similar

level as in the L-NNA studies via constriction of the thoracic descending aorta and brachiocephalic trunk using adjustable snares. Recordings of 20 s duration were digitized at 500 Hz under baseline conditions, and after haemodynamics had stabilized after each intervention. At the end of the study, animals were killed with an overdose of pentobarbitone sodium (100 mg kg^{-1}).

Data analysis

Experimental data were analysed with a custom script written in Spike2 (Cambridge Electronic Design, Cambridge, UK). Signals were low pass filtered (cut-off 48 Hz) to remove electrical interference and beat onset was defined as the time when LV pressure began to rise, detected via signal curvature according to a validated algorithm (Mynard *et al.* 2008). Analysis was performed on ensemble-averaged data derived from at least 10 individual beats.

For WIA, mean blood velocity (U) was estimated from measured flow and cross-sectional area derived from the flow probe diameter (Hollander *et al.* 2001; Penny *et al.* 2008). Proximal circumflex coronary blood pressure (at the location of flow measurement) was assumed to be identical to ascending aortic blood pressure (Pijls *et al.* 2000; Brosh *et al.* 2002), aside from a small time delay determined by aligning the early systolic upstroke of pressure and coronary flow. Blood density (ρ) was assumed to be 1.05 g cm^{-3}. Wave speed (c) was calculated via the PU-loop method for the aorta (Khir *et al.* 2001) and via the sum of squares method for the circumflex coronary artery (Davies *et al.* 2006*b*).

Coronary vascular resistance was calculated as [mean aortic pressure − mean left atrial pressure]/mean circumflex artery (Cx) flow. To define the association between the coronary BDW$_{dia}$ and myocardial relaxation, the peak negative rate of change of LV pressure (LV dP/dt_{min}) and the time constant of relaxation (τ) were calculated (Mirsky, 1984). The latter was obtained by fitting the equation LVP $= a_1 \exp[-(t - t_0)/\tau] + a_0$ to LV pressure (LVP), where a_0 and a_1 are fit coefficients, t_0 is the time of dP/dt_{min} and the fit was performed between t_0 and the time at which pressure had dropped to a value of $P_{min} + 0.1(P_{dpdtmin} - P_{min})$, where P_{min} and $P_{dpdtmin}$ are the minimum diastolic pressure and the pressure at dP/dt_{min}.

Statistical analysis

Statistical analysis of the experimental data was performed with the MATLAB and Statistics Toolbox 2016a (The MathWorks, Inc., Natick, MA, USA). Data were tested for normality using the Lilliefors test and logarithmically transformed when non-normal. When comparing wave magnitude between aortic and coronary arterial sites, wave intensities were normalized to the peak intensity of the FCW$_{sys}$ in the respective site. Comparisons were performed with repeated measures one-way analysis of variance. Simple and stepwise multiple linear regression with pooled data was used to test for correlations between BDW$_{dia}$ magnitude and (i) LV dP/dt_{min}, (ii) LV τ and (iii) aortic FDW$_{dia}$. Strength of correlation is reported as adjusted R^2 and interpreted as strong ($0.5 < R^2 \leq 1$), moderate ($0.3 < R^2 \leq 0.5$), weak ($0.1 < R^2 \leq 0.3$) or very weak ($R^2 \leq 0.1$). Data are reported as mean $\pm$ standard deviation, with significance defined as $P < 0.05$.

Results

Model-derived data

Simulated pressure, flow and wave intensity signals in the aorta and coronary artery of the virtual older adult human are shown in Fig. 5. The coronary wave intensity profile contains all of the waves commonly identified in clinical studies, and the relative timing and magnitude of the respective waves is representative of published clinical data (Davies *et al.* 2006*a*). Importantly, the coronary FDW$_{dia}$ is almost half the size of the aortic FDW$_{dia}$, relative to the FCW$_{sys}$, whereas a prominent coronary FCW$_{dia}$ is present despite a negligibly small aortic FCW$_{dia}$.

Figure 6 shows the effects of preventing all aortic waves from passing into the coronary arteries. This abolished both the coronary FCW$_{sys}$ and BCW$_{sys}$, indicating that the BCW$_{sys}$ arises solely from reflection of the FCW$_{sys}$. The FDW$_{dia}$ was also abolished as expected, but not the FCW$_{dia}$, with the remaining wave (designated FCW$_{ref}$) clearly arising from negative reflection of the BDW$_{mr}$, just as the FDW$_{ic}$ arises from negative reflection of the BCW$_{ic}$. The remaining BDW$_{mr}$ peak was 69% smaller than the BDW$_{dia}$, consistent with a contribution of wave reflection to the BDW$_{dia}$ (keeping in mind that the reflected wave adds non-linearly to BDW$_{mr}$).

Figure 7 shows wave intensity profiles in a series of simulations in which a variable time delay (t_d) was applied to waves entering the coronary arteries from the aorta, where $t_d = 0$ corresponds to the reference simulation (noting that only the late systolic and early-to-mid diastolic periods are shown); Fig. 8 shows the corresponding peak intensity and cumulative intensity of observed waves *versus* t_d. With a large negative or positive delay, an ensemble of three waves related to changes in aortic pressure are seen, namely the FDW$_{A \rightarrow C}$, which is reflected as a BDW$_{ref}$, then re-reflected as a forward compression wave, referred to as FCW$_{ref1}$. This wave ensemble shifts with changing t_d, whereas the two waves arising distally from myocardial relaxation are fixed (BDW$_{mr}$ and its reflected wave, FCW$_{ref2}$). Importantly, when $-20 \leq t_d \leq 30$ ms, the BDW$_{ref}$ and BDW$_{mr}$ overlap and only a single combined wave

(BDW$_{dia}$) is apparent, which is substantially larger (peak intensity 0.76 × 10^6 W m^{-2} s^{-2}) than the sum of the BDW$_{ref}$ and BDW$_{mr}$ waves in isolation (0.44 × 10^6 W m^{-2} s^{-2}). Similarly, when the FCW$_{ref1}$ and FCW$_{ref2}$ overlap, the combined single wave (FCW$_{dia}$) is larger (0.74 × 10^6 W m^{-2} s^{-2}) than the sum of the two component waves in isolation (0.31 × 10^6 W m^{-2} s^{-2}). Finally, a cancelling effect of FCW$_{ref2}$ on FDW$_{A \to C}$ led to a resultant FDW$_{dia}$ that was up to 97% smaller than the FDW$_{A \to C}$. However, even when this cancellation was maximal (at t_d = 30 ms), a prominent contribution of BDW$_{ref}$ remained (black arrow in Fig. 7).

Based on the simulations in Fig. 7, BDW$_{mr}$ accounted for 74% of the BDW$_{dia}$ (peak intensity), which was similar to the value of 80% estimated from the reference simulation (t_d = 0) via eqn (7); the contribution of wave reflection was thus underestimated by 6%. Figure 9A shows that coronary reflection index was higher during systole than diastole (difference of 0.08), as expected given the higher coronary impedance during systole. However, this value was almost identical during the early systolic and early diastolic periods in the proximal LAD (0.21 and 0.22 respectively, see shaded bars in Fig. 9A). Further analysis revealed that the time variation of proximal LAD reflection index was similar to the resistance variation of resistance arteries (R_1) in the intramyocardial circulation (Fig. 9B, showing data for the terminal LAD segment,

where R_1 is the parallel sum from the three transmural layers, cf. Fig. 4C). Combining data from all terminal arteries supplying the LV free wall and septum, R_1 was 12 ± 3% higher ($P < 0.001$) during the early diastolic period ('dia') than early systolic ('sys') period (Fig. 9C), leading to a 9 ± 8% higher reflection index during early diastole ($P < 0.001$, Fig. 9D).

As shown in Fig. 10, the contribution of myocardial relaxation to BCW$_{dia}$ displayed minor sensitivity to changes in aortic mean pressure, intramyocardial compliance, coronary wave speed and monitoring location along the LAD; moderate sensitivity to aortic pulse pressure; and high sensitivity to intramyocardial resistance (R_1). Overall, estimation of this contribution via eqn (7) was 6 ± 5% higher than the actual contribution obtained via the wave shifting approach. These results support the applicability of eqn (7) and suggest that small differences in reflection index between early systole and early diastole are likely to cause minor overestimation and underestimation of the contributions of myocardial relaxation and wave reflection respectively.

The difference between true coronary FDW$_{A \to C}$ (based on simulations in Fig. 7) and that estimated from eqn (4) (when t_d = 0) was less than 5%. True coronary FCW$_{A \to C}$ could not be ascertained for comparison with eqn (5) due to re-reflection of the BDW$_{ref}$ at the coronary ostium.
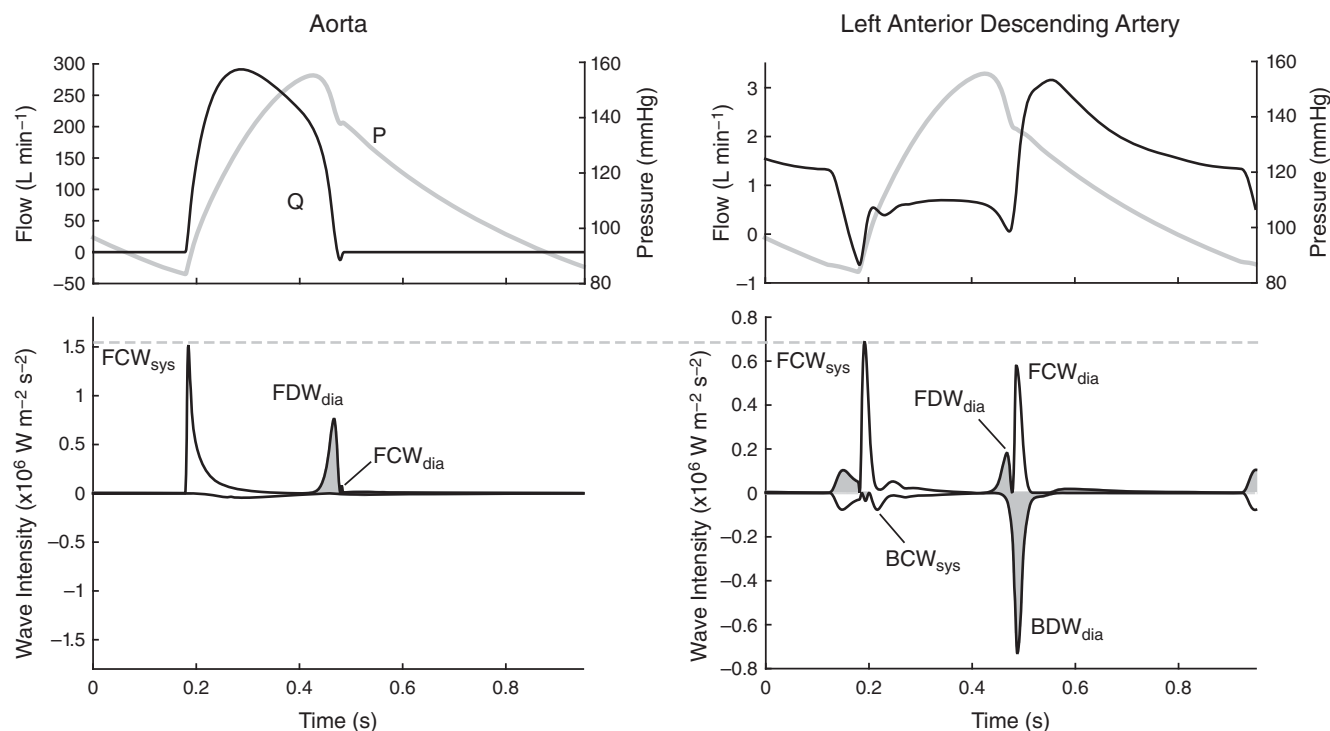

Figure 5. Pressure (P), flow (Q) and wave intensity from the aorta and proximal left anterior descending artery (LAD) of the computational model
Decompression waves are shaded.

In vivo data

Haemodynamics. A summary of relevant haemodynamic data is provided in Table 1. Heart rate and cardiac output decreased after L-NNA ($P < 0.05$) but did not change with aortic constriction. Systolic blood pressure increased by a similar amount with L-NNA and aortic constriction ($P = 0.13$) but was related to an increase in mean pressure in the former and pulse pressure in the latter. Cx flow was similar in both groups at baseline ($P = 0.7$) but increased more with aortic constriction than L-NNA (by 26.5 ± 9.8 *vs.* 13.7 ± 12.3 mL min^{-1}, $P = 0.03$) despite a higher diastolic pressure with L-NNA ($P = 0.03$, Table 1). Coronary vascular resistance increased by ~30% after L-NNA ($P = 0.04$) but did not change with aortic constriction ($P = 0.28$). LV dP/dt_{min} and τ were similar in both groups at baseline ($P > 0.5$) and displayed similar ($P > 0.3$) changes with afterload increase.

Systolic waves. Wave intensity data are summarized in Table 2 and a representative example is shown in Fig. 11. Results are here discussed in relation to peak intensity unless otherwise stated, but similar findings pertain to cumulative intensity (Table 3). Aortic (Ao) and Cx FCW$_{sys}$ decreased substantially with L-NNA ($P < 0.004$) but did not change with aortic constriction ($P = 0.7$). The concept that Cx BCW$_{sys}$ arises from reflection of the Cx FCW$_{sys}$ was supported by a strong correlation between these waves ($R^2 = 0.62$; $P < 0.001$), along with a relatively consistent delay of 23.9 ± 6.6 ms that did not change with increased afterload ($P > 0.4$). Moreover, the reflection index Cx BCW$_{sys}$/FCW$_{sys}$ (0.26 ± 0.20 at baseline) more than doubled after L-NNA infusion ($P < 0.001$), but was unaffected by aortic constriction ($P = 0.8$).

Diastolic waves. Large differences in the relative intensity of early-diastolic forward waves were found when comparing Ao and Cx sites (Fig. 12). After normalization to FCW$_{sys}$, Cx FDW$_{dia}$ was smaller than Ao FDW$_{dia}$ in every recording (by 40 ± 16% overall), whereas Cx FCW$_{dia}$ was always much larger than Ao FCW$_{dia}$ (by 512 ± 373%).

The estimated Cx BDW$_{ref}$ almost doubled with L-NNA ($P = 0.007$) but did not increase significantly with aortic constriction ($P = 0.12$). Cx BDW$_{mr}$ accounted for only ~30% of the measured BDW$_{dia}$ at baseline (eqn 8), with a trend for this contribution to decrease after LNNA (to 13%, $P = 0.09$, Table 2).

With simple linear regression, no correlation was detected between Cx BDW$_{dia}$ and LV τ ($R^2 < 0.1$, $P > 0.05$, Fig. 13, left panels), but a weak-to-moderate correlation was found between normalized Cx BDW$_{dia}$ magnitude and LV dP/dt_{min} ($R^2 = 0.3$, $P \le 0.001$, Fig. 13, middle panels).
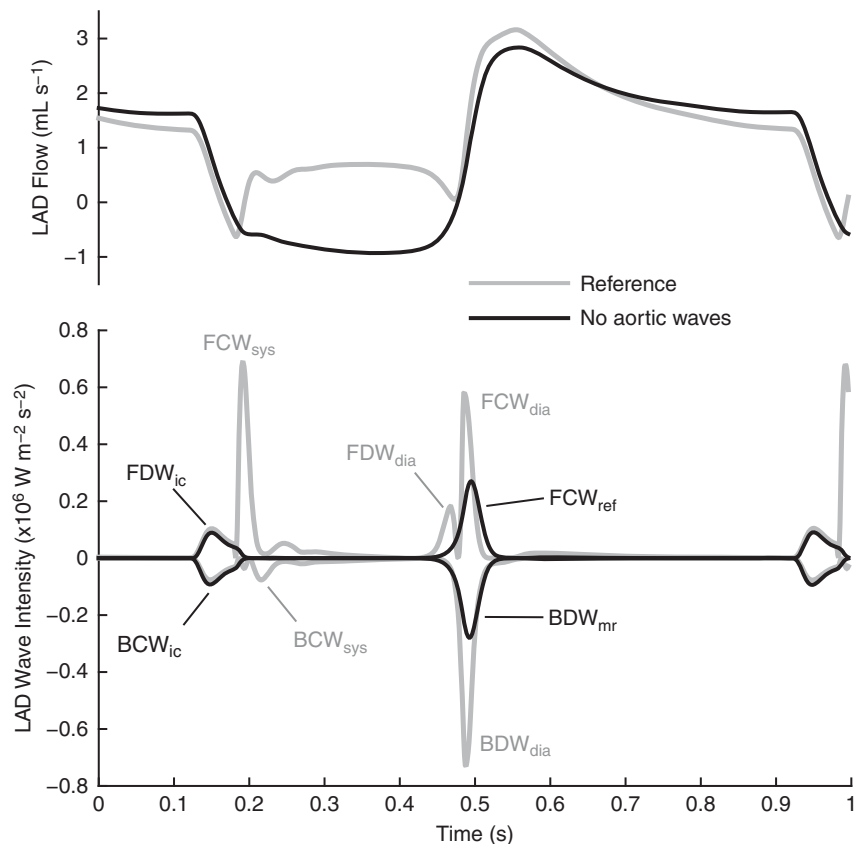

Figure 6. Results of a virtual experiment in which all aortic waves were prevented from passing into the coronary arteries
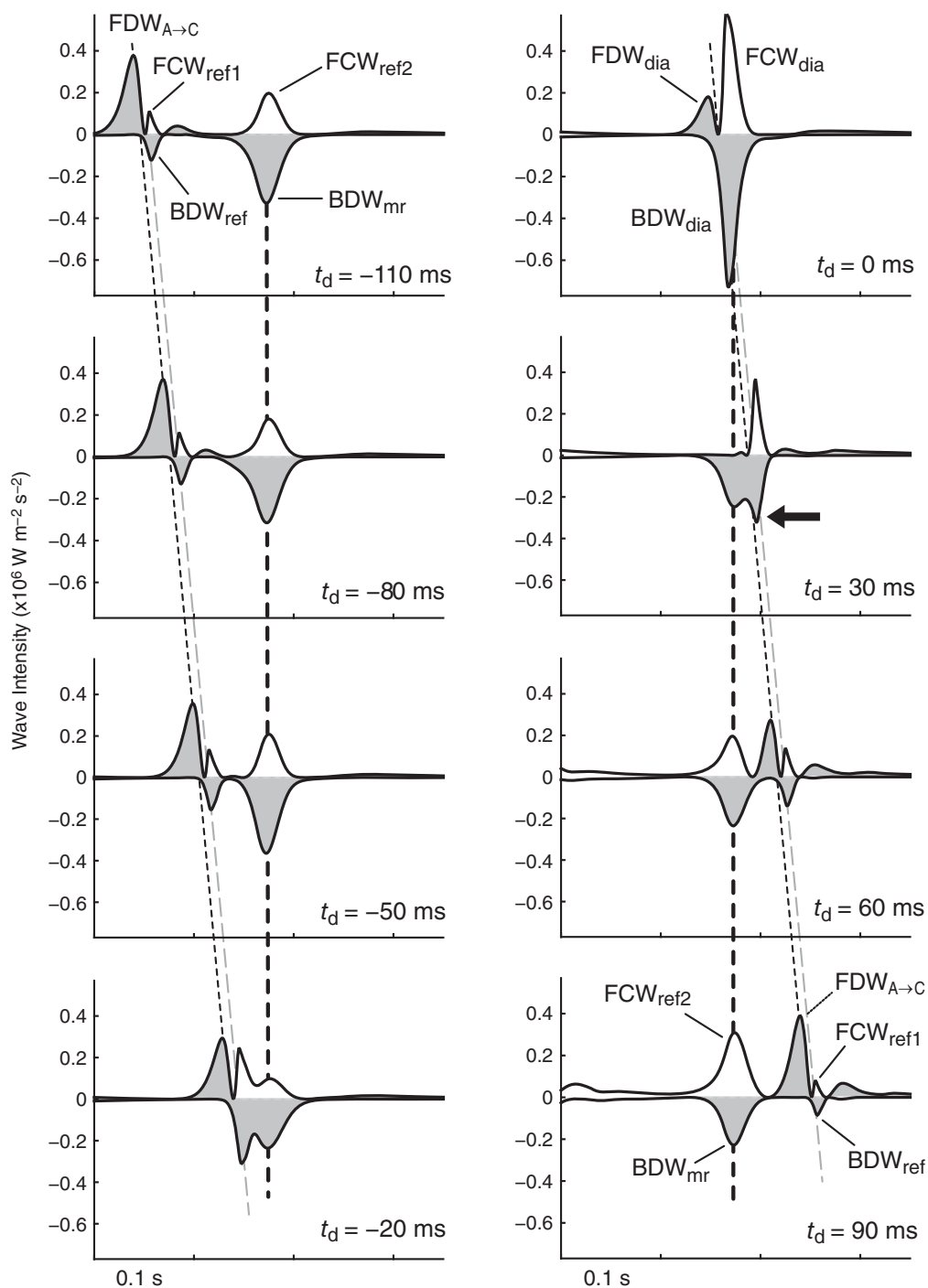
Figure 7. Results of a virtual experiment in which coronary ostial pressure was shifted with a variable time delay (t_d), revealing the mechanistically distinct waves that combine (i.e. add or subtract) non-linearly when aligned (selected time points are displayed from 23 simulations)

The initial ensemble of three waves seen when $t_d \leq -50$ ms arise from the passage of a forward decompression wave from the aorta into the coronary arteries (FDW$_{A \to C}$), and its distal reflection (BDW$_{ref}$) and proximal re-reflection (FCW$_{ref1}$). The BDW$_{mr}$ arises from a distal suction effect and is then reflected proximally (FCW$_{ref2}$). The reference case shown in Fig. 5 corresponds to $t_d = 0$. Dashed lines indicate the times of peak FDW$_{A \to C}$ (thin black line), BDW$_{ref}$ (grey line) and BDW$_{mr}$ (thick black line). Decompression waves are shaded.

Conversely, a strong correlation was found between Cx BDW_{dia} and Ao FDW_{dia} ($R^2 > 0.6$, $P < 10^{-7}$, Fig. 13, right panels). Upon multiple linear regression analysis, LV dP/dt_{min} did not provide additional predictive value over Ao FDW_{dia} ($P = 0.4$), again suggesting that reflection of $FDW_{A \to C}$ made a greater contributor to BDW_{dia} than distal suction effects.

Discussion

A skilled magician uses smoke and mirrors to conceal, exaggerate and mislead. This study uncovered a phenomenon whereby coronary wave reflection acts in a similar way, obscuring the true influence of active upstream and downstream forces on early diastolic waves in conduit arteries. Specifically, although distal myocardial relaxation generates a backward-running decompression (or 'suction') wave, as is currently believed (Davies *et al.* 2006*a*), distal reflection of a forward decompression wave can have a major 'exaggerating' effect on the measured backward wave (BDW_{dia}), due to a non-linear wave addition phenomenon. Moreover, near-complete negative reflection of the BDW_{dia} at the coronary ostium produces a forward compression wave (FCW_{ref}) that conceals the aortic FDW_{dia} and exaggerates the aortic FCW_{dia} when viewed from the coronary arteries.

While an oft-stated benefit of coronary wave intensity is that it allows clear assessment of upstream and downstream processes (Siebes *et al.* 2009; Lu *et al.* 2011; Kyriacou *et al.* 2012; Rolandi *et al.* 2012; Claridge *et al.* 2015; Lee *et al.* 2016; Raphael *et al.* 2016), a key conclusion of this study is that, mechanistically, both upstream and downstream processes can have a significant effect on the magnitude of both forward and backward waves (directly and via wave reflection). However, with additional knowledge of aortic wave intensity, we have described a novel method to unmask the effect of wave reflection and recover information about upstream and downstream forces (such as distal suction) on early-diastolic coronary waves.

Wave reflection in coronary arteries

Limited information exists about wave reflection in coronary arteries. Rumberger *et al.* (1979) posited wave reflection as an explanation for prominent pressure and velocity oscillations observed in distal coronary arteries of the horse, while Arts *et al.* (1979) concluded that, in dogs, frequencies below 7 Hz are reflected at the coronary peripheral resistance, whereas higher frequencies undergo minimal reflection. The study by Arts *et al.* (1979), and in particular a recent detailed morphometric and theoretical study by Rivolo *et al.* (2016), suggested that the major
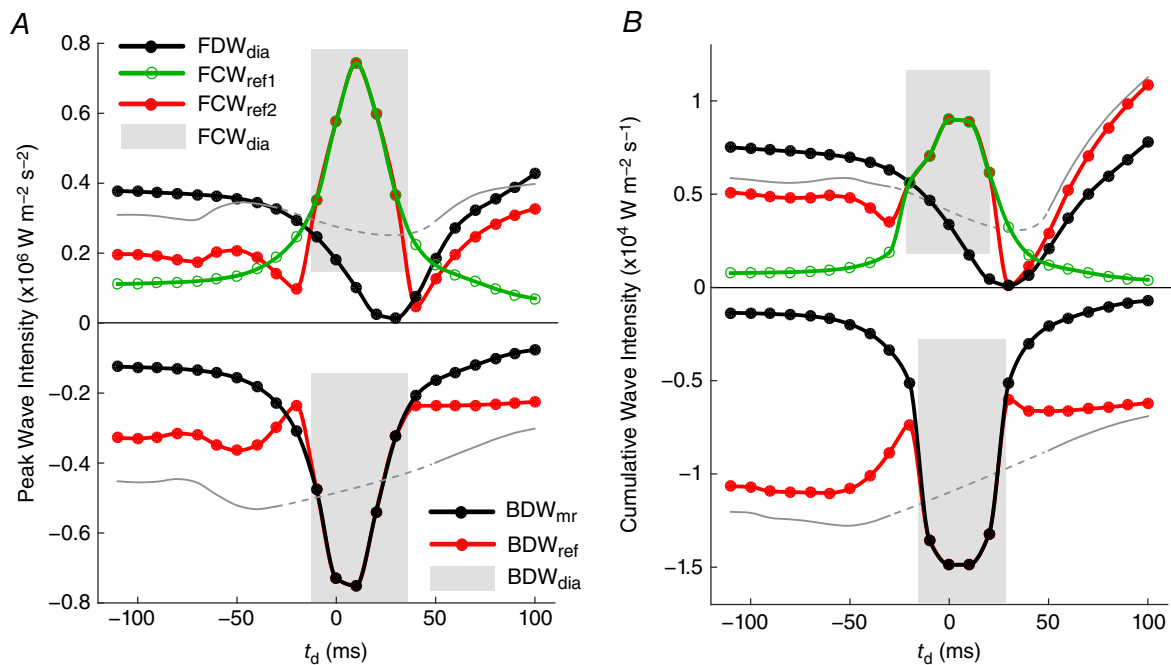

Figure 8. Peak intensity and cumulative intensity of forward and backward waves shown in Fig. 7 *versus* the delay time (t_d)
Shaded areas indicated where two waves overlap and appear as a single wave peak. Thin grey lines indicate the *linear* sum $FCW_{ref1} + FCW_{ref2}$ (top) or $BDW_{mr} + BDW_{ref}$ (bottom), while the dashed segments indicate an approximate interpolation; these may be compared with the observed wave magnitude, which results from *non-linear* summation. Note that $FDW_{A \to C}$ in Fig. 7 refers to FDW_{dia} in the absence of interactions with reflected waves. [Colour figure can be viewed at wileyonlinelibrary.com]

conduit coronary arteries are relatively well matched in the forward direction, as was assumed in the design of our 1D model. This implies that wave reflection occurs mainly in the small resistance arteries.

Davies *et al.* (2006a) proposed reflection of FCW_{sys} as a likely mechanism underlying the BCW_{sys}. This was supported by our modelling study, in which blocking the aortic FCW_{sys} from passing into the coronary arteries abolished the BCW_{sys} (Fig. 6). Further support for this interpretation was provided by experimental data showing a strong correlation between BCW_{sys} and FCW_{sys}, a consistent delay between these waves and a wave intensity-based reflection index that increased dramatically with coronary vasoconstriction.

Along with distal reflection, Davies *et al.* (2006a) also proposed that backward-running waves arriving at the coronary ostium are likely to undergo near-complete negative reflection, due to the large impedance decrease at this junction. Hence, during isovolumic contraction, an FDW_{ic} was postulated to arise from negative reflection

of the BCW_{ic}; this explanation was supported by our virtual experiments in which preventing aortic waves from passing into the coronary arteries did not affect FDW_{ic} (Fig. 6).

In contrast to its recognized major influence during early systole, however, the potential role of wave reflection in modulating the coronary wave intensity profile during early diastole has largely been ignored until the present study.

Early-diastolic backward decompression wave (BDW_dia)

The BDW_{dia} is considered the most important coronary wave physiologically, as it appears to be the primary actuator of diastolic coronary blood flow and is influenced by factors such as ageing, exercise, aortic stenosis, LV hypertrophy, coronary stenosis and myocardial resynchronization therapy (Davies *et al.* 2006*a*; Kyriacou *et al.* 2012; Lockie *et al.* 2012; De Silva *et al.* 2013;
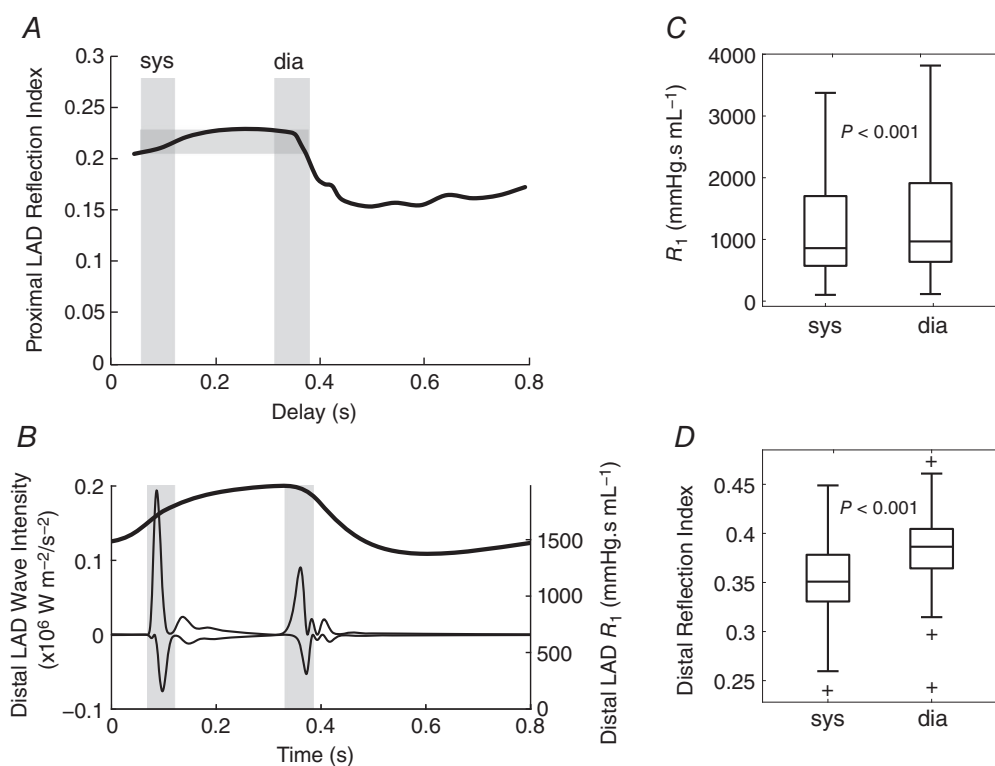

Figure 9. Assessment of the variation in model-based reflection index over the cardiac cycle, obtained by setting the intramyocardial pressure source (p_{im} in Fig. 4C) to zero but retaining the p_{im}-related changes in intramyocardial resistance (R_1, R_m, R_2 in Fig. 4C)
A, reflection index calculated from BCW_{sys}/FCW_{sys} cumulative intensity ratio in the proximal left anterior descending artery (LAD), with intra-cycle variations obtained by introducing delays in coronary ostial pressure and hence the timing of incident waves (delay time based on peak BCW_{sys}). Grey bars indicate the early systolic period (sys) and early diastolic period (dia), which span from the start of the incident wave to the end of the reflected wave. *B*, wave intensity at the end of the terminal LAD segment and time-varying R_1 (parallel combination from all layers) in the connecting 0D microcirculation compartment. *C* and *D*, time-averaged R_1 during the 'sys' and 'dia' periods (*C*), and reflection index calculated from the local incident and reflected waves (*D*), obtained from all terminal 1D segments supplying the left ventricular free wall and septum.

Claridge *et al.* 2015; Narayan *et al.* 2015). The BDW_{dia} is currently interpreted as arising solely from a suction effect within the coronary microcirculation, as the relaxing myocardium releases the external (intramyocardial) pressure developed during systole (Davies *et al.* 2006*a*; Kyriacou *et al.* 2012; Narayan *et al.* 2015). Lee *et al.* (2016) investigated the sensitivity of the major coronary waves to several key parameters in their model and found a dependence of BDW_{dia} on myocardial relaxation rate and degree of dysynchrony, consistent with the distal suction mechanism; however, a possible contribution of wave reflection was not explored.

Our experimental and computational data provide strong evidence that wave reflection makes an important contribution to the BDW_{dia}. In the computational model, preventing aortic waves from passing into the coronary arteries caused BDW_{dia} amplitude to fall by 69%, suggesting a contribution of reflection to this wave. In the experimental data, a strong correlation was found between the size of the incident wave ($FDW_{A \to C}$) and BDW_{dia} ($R^2 > 0.6$), but there was no correlation with LV τ and only a weak-to-moderate correlation with LV dP/dt_{min} ($R^2 = 0.3$) that lost significance in a multivariate model. Previous studies have reported R^2 values of $0.21-0.35$ between LV dP/dt_{min} and the coronary BDW_{dia}, in agreement with our findings (Kyriacou *et al.*

2012; Ladwiniec *et al.* 2016), although Ladwiniec and colleagues also reported a correlation ($R^2 = 0.35$) between LV τ and BDW_{dia} (Ladwiniec *et al.* 2016).

A surprising finding of our study was that the distal suction mechanism (i.e. BDW_{mr}) accounted for only 30% of the measured BDW_{dia} in the experimental study, and hence wave reflection appeared to be the dominant mechanism. Moreover, coronary vasoconstriction with L-NNA increased the reflection-related wave (BDW_{ref}) and tended to reduce the contribution of distal suction (see Table 2). However, these data in healthy, young sheep contrasted with the computational model representing an older, hypertensive human in which the distal suction mechanism was dominant, accounting for ~75% of the BDW_{dia}. The contribution of distal suction to BDW_{dia} may therefore be quite variable and influenced by a variety of (patho)physiological factors; these should be investigated in more detail in future studies.

We showed for the first time that, due to the definition of wave intensity as $dPdU$, the addition of two mechanistically distinct waves is non-linear. In other words, when BDW_{ref} and BDW_{mr} combine, the resultant wave (BDW_{dia}) is substantially greater than simply $BDW_{ref} + BDW_{mr}$ (by ~60% at baseline in our sheep studies). This may partly explain why the BDW_{dia} is so prominent in many published figures, much more so
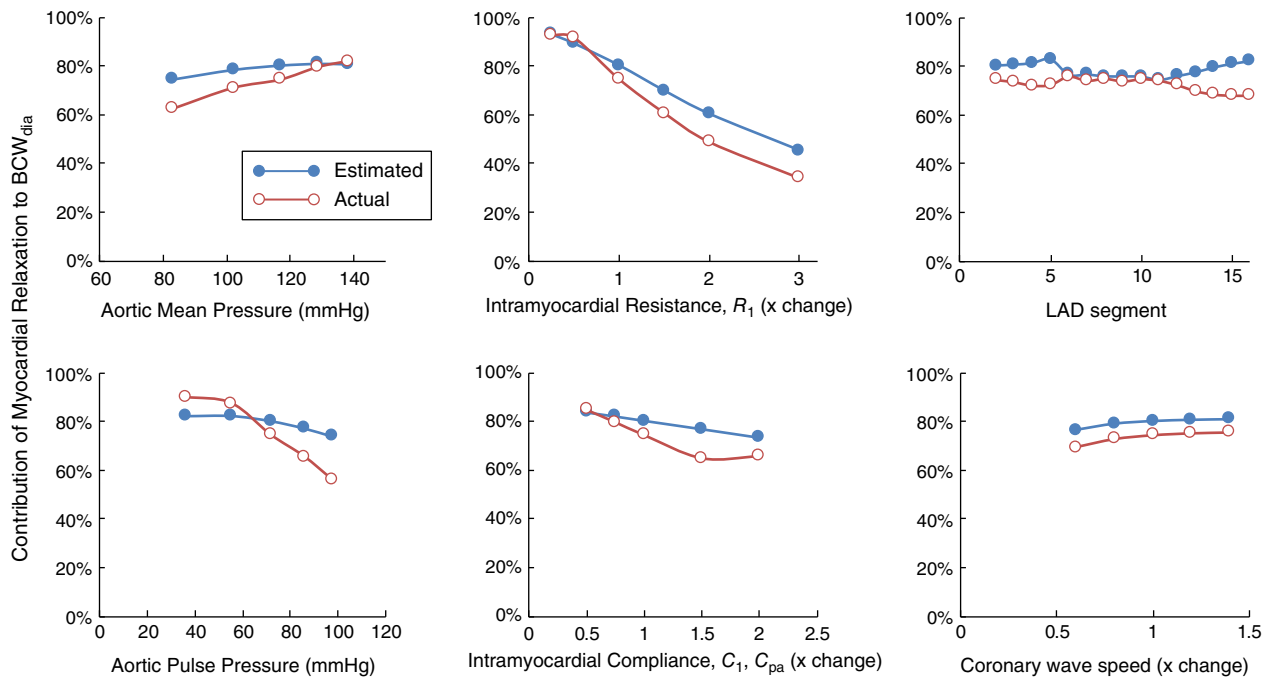
Figure 10. Model sensitivity analysis of key variables to the percentage contribution of myocardial relaxation to the BCW_{dia}

Aortic mean and pulse pressures were adjusted by varying systemic vascular resistance and aortic wave speed respectively. Intramyocardial resistance (R_1) and compliances (C_1 and C_{pa}) are indicated in Fig. 4*C*. 'LAD segment' refers to the 1D segment numbers shown in Fig. 4*A*. 'Estimated' refers to values estimated via eqn (7) and 'actual' refers to values obtained by shifting ostial pressure by -60 ms, which separates the BDW_{mr} and BDW_{ref} (cf. Fig. 7). [Colour figure can be viewed at wileyonlinelibrary.com]

Table 1. Haemodynamic data for the *in vivo* experiments

	L-NNA group (n = 11)		Constriction group (n = 7)	
	Baseline	L-NNA	Baseline	Aortic constriction
Heart rate (bpm)	110 ± 14	100 ± 14[a]	105 ± 17	111 ± 17
Cardiac output (L min^{-1})	3.12 ± 0.68	2.56 ± 0.44[a]	3.07 ± 0.65	3.67 ± 0.88
Cx flow (mL min^{-1})	29.5 ± 11.6	43.2 ± 17.7[b]	32.1 ± 16.1	58.6 ± 19.9[c]
Cx effective vascular resistance (mmHg.min mL^{-1})	2.44 ± 1.18	3.13 ± 1.60[a]	2.37 ± 0.99	2.13 ± 0.80
Ao systolic BP (mmHg)	75.5 ± 7.7	134.5 ± 11.9[c]	79.5 ± 7.6	147.4 ± 7.6[c]
Ao mean BP (mmHg)	66.3 ± 9.1	123.9 ± 11.2[c]	70.5 ± 9.2	121.8 ± 8.8[c]
Ao diastolic BP (mmHg)	58.1 ± 10.0	115.5 ± 10.6[c]	62.4 ± 10.5	103.0 ± 11.4[c]
Ao pulse BP (mmHg)	17.4 ± 3.9	19.0 ± 2.6	17.0 ± 4.3	44.3 ± 9.9[c]
LV dP/dt$_{min}$ (mmHg s^{-1})	−1195 ± 191	−1878 ± 370[c]	−1271 ± 294	−2126 ± 443[c]
LV τ (ms)	27.8 ± 4.7	19.3 ± 4.6[c]	29.1 ± 5.9	21.5 ± 8.7[a]

Ao, aortic; BP, blood pressure; Cx, circumflex coronary artery; dP/dt$_{min}$, maximal rate of pressure fall; LV, left ventricular; τ, time constant of isovolumic relaxation.
[a]$P < 0.05$, [b]$P \leq 0.01$, [c]$P < 0.001$ compared with baseline.
Baseline variables between L-NNA and aortic constriction groups were not significantly different.

Table 2. Peak wave intensity for the *in vivo* study

	Baseline	L-NNA	Baseline	Aortic constriction
Systolic waves				
Ao FCW$_{sys}$	81.8 ± 55.9	19.1 ± 4.5[b]	86.5 ± 56.7	95.6 ± 43.7
Cx FCW$_{sys}$	14.6 ± 8.0	2.0 ± 1.1[c]	18.6 ± 11.1	20.7 ± 13.6
Cx BCW$_{sys}$	−3.1 ± 2.2	−1.1 ± 0.4[b]	−6.0 ± 5.1	−6.6 ± 5.8
Cx ∣ BCW$_{sys}$/FCW$_{sys}$ ∣	0.21 ± 0.08	0.64 ± 0.31[c]	0.35 ± 0.30	0.32 ± 0.14
Diastolic waves				
Ao FDW$_{dia}$	74.3 ± 18.3	106.6 ± 30.9[c]	86.8 ± 25.9	152.6 ± 81.2[a]
Ao FCW$_{dia}$	21.9 ± 14.1	28.0 ± 16.8	30.2 ± 29.6	27.7 ± 51.4
Cx FDW$_{dia}$	6.0 ± 3.0	5.3 ± 2.6	5.5 ± 2.3	9.2 ± 4.8
Cx FDW$_{A \to C}$ (eqn 4)	*14.9 ± 6.4*	*10.5 ± 5.5*	*17.9 ± 5.3*	*31.9 ± 22.2*
Cx FCW$_{dia}$	13.1 ± 5.7	16.0 ± 10.3	18.7 ± 13.5	15.8 ± 12.7
Cx FCW$_{A \to C}$ (eqn 5)	*3.9 ± 2.2*	*3.0 ± 2.6*	*6.7 ± 7.1*	*4.0 ± 5.4*
Cx BDW$_{dia}$	−8.5 ± 6.2	−10.3 ± 5.5	−13.2 ± 7.7	−22.8 ± 17.1
Cx BDW$_{ref}$ (eqn 6)	*−3.2 ± 1.9*	*−5.7 ± 1.9[b]*	*−5.5 ± 4.1*	*−9.7 ± 7.5*
Cx BDW$_{mr}$ (eqn 7)	*−2.2 ± 3.3*	*−1.1 ± 1.4*	*−2.5 ± 2.7*	*−3.2 ± 2.6*
Cx BDW$_{mr}$ /(BDW$_{mr}$ + BDW$_{ref}$)	30 ± 34%	13% ± 16%	31 ± 27%	24 ± 21%

Time-corrected wave intensity units: 10^4 W m^{-2} s^{-2}.
[a]$P < 0.05$, [b]$P \leq 0.01$, [c]$P < 0.001$ compared with the respective baseline.
Items in italics refer to component waves that were estimated via the indicated equation. There were no significant differences between baselines of L-NNA and aortic constriction groups for any quantity.

than the BCW$_{ic}$ despite *in vivo* data suggesting that intra-myocardial pressure rises (during isovolumic contraction) and falls (during isovolumic relaxation) at a similar rate (Rabbany *et al.* 1989). An important implication of this non-linear addition principle is that any delay between BDW$_{ref}$ and BDW$_{mr}$ may substantially influence the intensity of the combined or partially combined wave (e.g. compare $t_d = -20$ ms and $t_d = 0$ ms in Fig. 7). That the BDW$_{ref}$ and BDW$_{mr}$ may not always be aligned is suggested by numerous published figures in which multiple BDW peaks are evident in the early diastolic period, although this could also be due to other factors such as dyssynchronous relaxation (Hadjiloizou *et al.* 2008; Davies *et al.* 2011; Kyriacou *et al.* 2012; Lu *et al.* 2012; De Silva *et al.* 2014; Broyd *et al.* 2016; Raphael *et al.* 2016).

Early-diastolic forward decompression wave (FDW$_{dia}$)

Based on the seminal work of Parker *et al.* (1988), the FDW$_{dia}$ is widely regarded as the second major wave in

the aortic wave intensity profile and is associated with a fall in pressure and flow prior to valve closure. An FDW_{dia} also appears in the coronary wave intensity profile and is believed to arise from transmission of the aortic FDW_{dia} into the coronary arteries (Davies *et al.* 2006*a*). However, we found that the coronary FDW_{dia} was ∼60% smaller (peak intensity, after normalization to FCW_{sys}) than the aortic FDW_{dia}. Closer inspection revealed that the FDW entering the coronary arteries from the aorta ($FDW_{A\to C}$) is partially cancelled by negative reflection of the BDW_{dia} at the coronary ostium (see Fig. 3*B*). Such reflection produces a forward compression wave (FCW_{ref}) which has a cancelling/concealing effect on the $FDW_{A\to C}$.

Introduction of a variable delay between aortic-originating waves and distally generated waves in a virtual experiment indicated that this cancelling effect can cause the $FDW_{A\to C}$ to essentially disappear under certain circumstances (Fig. 7). It is tempting to conclude that if the measured coronary FDW_{dia} is small or even absent, wave reflection must make a negligible contribution to the BDW_{dia}. However, we found that a prominent BDW_{ref} may still be present in such circumstances, apparently because the BDW_{ref} arises from reflection of the concealed $FDW_{A\to C}$ (see $t_d = 30$ ms in Fig. 7). For this reason, the true influence of wave reflection on the BDW_{dia} should be assessed with respect to $FDW_{A\to C}$ as the incident wave, rather than FDW_{dia}.

Diastolic forward compression wave (FCW_{dia})

An aortic FCW_{dia} arises from the transitory increase in pressure and flow associated with the dicrotic notch as the valve closes. This wave is also commonly observed in the coronary arterial wave intensity profile (Davies *et al.* 2006*a*; Hadjiloizou *et al.* 2008; Kyriacou *et al.* 2012; Lu *et al.* 2012; Ladwiniec *et al.* 2016; Raphael *et al.* 2016) and has been interpreted to arise from transmission of the aortic FCW_{dia} into the coronary arteries (Davies *et al.* 2006*a*; Narayan *et al.* 2015). However, inspection of published figures from these two locations suggest that the FCW_{dia} is generally more prominent in coronary arteries (Davies *et al.* 2006*a*; Kyriacou *et al.* 2012; Lu *et al.* 2012; Sinclair *et al.* 2015; Raphael *et al.* 2016) than in the aorta (Parker & Jones, 1990; Jones *et al.* 2002; Khir & Parker, 2005; Penny *et al.* 2008; Lu *et al.* 2012). Consistent with this impression, our comparison of concurrent aortic and coronary wave intensity profiles indicated that the coronary FCW_{dia} peak intensity was 2–21 times higher than aortic FCW_{dia}, relative to FCW_{sys} (see Fig. 12); in the computational studies, aortic FCW_{dia} was of negligible size but the coronary FCW_{dia} was very prominent (see Fig. 5).

The combination of experimental and computational data suggested that two mechanisms contributed to the FCW_{dia}. As expected, the first was transmission of the aortic FCW_{dia} into coronary arteries. However, the second
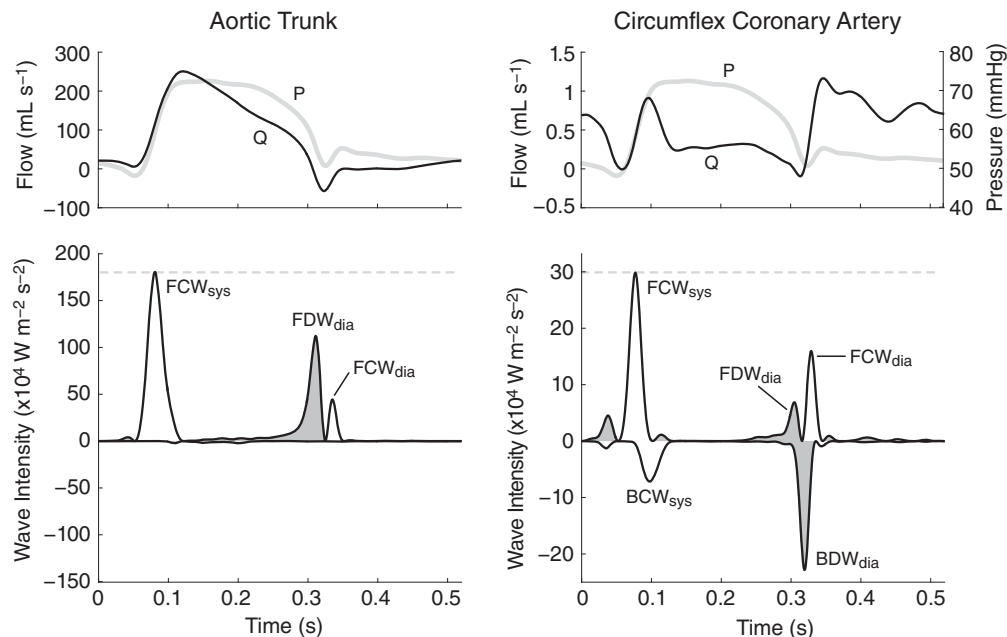

Figure 11. Representative example of simultaneously acquired wave intensity in the sheep aortic trunk (left) and circumflex coronary artery (right) in relation to blood pressure (P) and flow (Q) waveforms
High-fidelity pressure was measured in the aortic trunk and was assumed to be the same as circumflex coronary pressure (aside from a time offset applied to align early-systolic pressure and flow upstrokes). Wave abbreviations: BCW, backward compression wave; BDW, backward decompression wave; FCW, forward compression wave; FDW, forward decompression wave. Decompression waves are shaded. The main waves occur during early systole ('sys') and early diastole ('dia').

Table 3. Cumulative wave intensity (i.e. area under the wave)

	Baseline	L-NNA	Baseline	Aortic constriction
Systolic waves				
Ao FCW$_{sys}$	22.46 ± 12.86	9.81 ± 3.10[b]	24.93 ± 14.14	27.44 ± 9.02
Cx FCW$_{sys}$	2.83 ± 1.61	0.86 ± 0.40[b]	3.80 ± 2.08	4.23 ± 3.25
Cx BCW$_{sys}$	−0.81 ± 0.56	−0.53 ± 0.28	−1.42 ± 1.11	−1.47 ± 1.11
Cx | BCW$_{sys}$/FCW$_{sys}$ |	0.29 ± 0.11	0.61 ± 0.20[c]	0.39 ± 0.26	0.39 ± 0.20
Diastolic waves				
Ao FDW$_{dia}$	14.38 ± 3.52	18.57 ± 4.33[b]	16.86 ± 3.38	31.72 ± 11.27[b]
Ao FCW$_{dia}$	2.42 ± 1.51	2.69 ± 1.65	3.62 ± 3.41	2.36 ± 4.64
Cx FDW$_{dia}$	1.00 ± 0.51	0.70 ± 0.31[a]	0.92 ± 0.48	1.72 ± 1.16
Cx FDW$_{A→C}$ (eqn 4)	*1.93 ± 0.85*	*1.60 ± 0.56[a]*	*2.62 ± 1.30*	*4.68 ± 2.72*
Cx FCW$_{dia}$	1.62 ± 0.68	1.77 ± 1.11	2.32 ± 1.84	1.62 ± 1.38
Cx FCW$_{A→C}$ (eqn 5)	*0.30 ± 0.17*	*0.22 ± 0.17*	*0.64 ± 0.79*	*0.24 ± 0.37*
Cx BDW$_{dia}$	−1.95 ± 0.83	−2.10 ± 0.87	−2.60 ± 1.15	−4.80 ± 2.42[a]
Cx BDW$_{ref}$ (eqn 6)	*−0.57 ± 0.32*	*−0.95 ± 0.34[a]*	*−0.87 ± 0.51*	*−1.63 ± 1.16*

Cumulative wave intensity units: 10^3 W m^{-2} s^{-1}.
[a]$P < 0.05$, [b]$P \leq 0.01$, [c]$P < 0.001$ compared with the respective baseline.
Items in italics refer to component waves that were estimated via the indicated equation. There were no significant differences between baseline of Group 1 and baseline of Group 2 for any quantity. Note that BDW$_{mr}$ cumulative intensity cannot be calculated as for peak intensity.

and perhaps dominant mechanism was negative reflection of the BDW$_{dia}$ at the coronary ostium (FCW$_{ref}$), which was clearly demonstrated with a virtual experiment in which aortic waves were prevented from passing into the coronary arteries (see Fig. 6).

Overcoming the smoke and mirrors effect

A major conclusion of this study is that wave reflection obscures the true (i.e. wave reflection-independent) influence of upstream and downstream forces on the early diastolic forward and backward waves. However, by

making use of information from concurrent aortic wave intensity, we proposed novel techniques for estimating the reflection-independent waves that pass from the aorta into the coronary arteries (FDW$_{A→C}$ and FCW$_{A→C}$) and arise from distal suction effects (BCW$_{mr}$), as well as the reflection-related contribution to BDW$_{dia}$ (i.e. BDW$_{ref}$). *In silico* validation with our model suggested that these waves can be estimated with errors of less than 10%.

The proposed wave estimation techniques depend on several assumptions being satisfied. The first is that aorto-coronary wave transmission does not vary
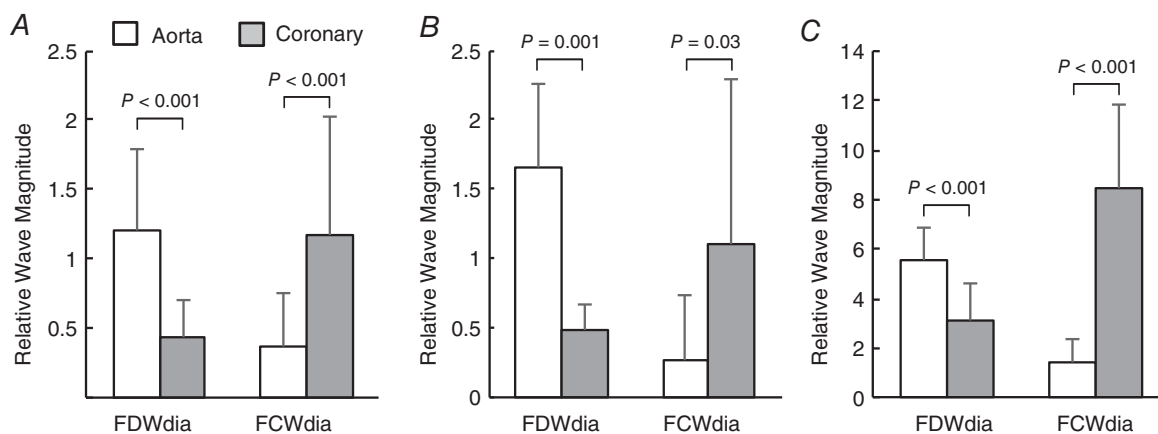

Figure 12. Comparison of early diastolic forward wave magnitude in the ascending aorta *vs.* the circumflex coronary artery at (*A*) baseline (all animals, *n* = 18), (*B*) after aortic constriction (*n* = 7) and (*C*) after administration of L-NNA (*n* = 11, note the difference in *y*-axis scale)
Peak wave intensities of FDW$_{dia}$ and FCW$_{dia}$ are expressed relative to that of FCW$_{sys}$ in the respective measurement location.

significantly between early systole and early diastole; indeed, based on transmission line theory, we calculated differences in transmission coefficient of less than 5% (Mynard *et al.* 2017). The second assumption (required for estimation of BDW_{ref} and BCW_{mr}) is that the coronary reflection coefficient is similar during early systole and early diastole (when FCW_{sys} and FDW_{dia} occur). When we tested this assumption using our model, we found that model-predicted reflection index was comparable to that in the experimental studies (0.21 *vs.* 0.29) and changed by less than 0.01 between early systole and early diastole (Fig. 9*A*). Model data also suggested that both intramyocardial resistance and distal reflection index were ~10% higher during early diastole than early systole (Fig. 9*B–D*), which, if anything, would tend to cause the contribution of wave reflection on BDW_{dia} to be underestimated.

Study limitations

This study had a number of limitations. Experimental studies were performed in healthy, young, anaesthetized open-chest sheep undergoing mechanical ventilation, and thus caution should be applied in extrapolating results to humans and other species with or without pathophysiology undergoing spontaneous respiration. While previous studies suggest that the anaesthetic alpha-chloralose has (Covert *et al.* 1989) or does not have (Cox, 1972) a vasoconstrictive effect, systemic vascular resistance at baseline in this study (21.9 ± 4.4 mmHg.L min^{-1}) was only slightly higher than the range 18.8–21.2 mmHg.L min^{-1} in chronically instrumented conscious sheep (Kemp *et al.* 1995) and effective circumflex coronary resistance in this study (2.4 ± 1.1 mmHg.min mL^{-1}) was the same as that derived from data in conscious sheep (Bednarik & May,
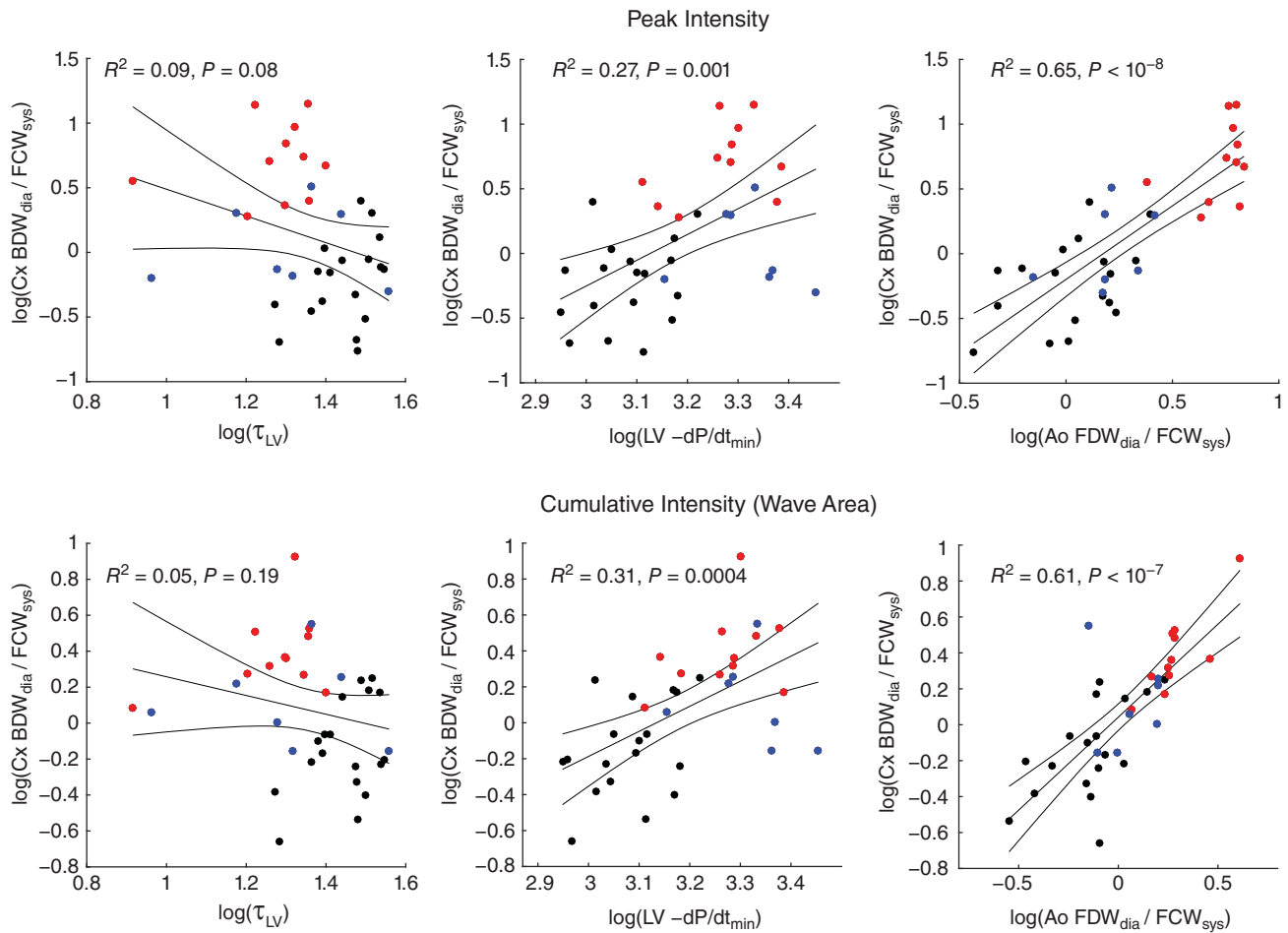

Figure 13. Linear regression analyses investigating relationships between the circumflex coronary (Cx) BDW_{dia} and LV isovolumic time constant (τ), LV dP/dt_{min} and aortic (Ao) FDW_{dia}, with wave magnitude quantified via peak wave intensity (top panels) and cumulative intensity (bottom panels) normalized to the respective FCW_{sys}
Data point colours (online version only) refer to baseline (black, both groups), L-NNA infusion (red) and aortic constriction (blue). [Colour figure can be viewed at wileyonlinelibrary.com]

1995; Parkes *et al.* 1997). However, we cannot exclude the possibility that some coronary vasoconstriction could have led to a greater influence of wave reflection on the BDW_{dia}, although any such effect is likely to be small.

The computational model is based on findings of many physiological studies from other research groups (Fisher *et al.* 1982; Spaan, 1985; Bruinsma *et al.* 1988; Rabbany *et al.* 1989; Dodge *et al.* 1992; Spaan *et al.* 2000; Algranati *et al.* 2010), has been validated in sheep (Mynard *et al.* 2014) and produced wave intensity profiles that were very consistent with published *in vivo* waveforms (Davies *et al.* 2006*a*). However, a number of factors were not accounted for in the model, such as the effects of cardiac motion (Ramaswamy *et al.* 2004), wave propagation effects in the microcirculation (Guiot *et al.* 1990) and the effects of external constraint on conduit arteries (Liu *et al.* 2008). The coronary microcirculation was modelled using lumped elements and simplifying assumptions were made about intramyocardial pressure. More detailed micro-vascular models, such as the poromechanical model described by Lee *et al.* (2016), may be useful for further investigating some of the issues raised in this paper.

While this study highlighted the complexity of coronary arterial wave dynamics, we did not study the effect of multiple re-reflections. In the sheep under baseline conditions, the magnitude of second- and third-generation waves would be expected to be in the order of ∼6% and ∼1.5% that of initial incident wave, not accounting for wave dispersion and dissipation. However, in cases where wave reflection is high (e.g. vasoconstriction or stenosis), these re-reflections may be more influential. Use of the theoretical framework described in this paper could be used in future to investigate these wave dynamics in even greater detail, although the limited fidelity of experimental data may make this challenging. We also did not investigate issues related to the 'windkesselness' of the coronary arterial network, which can lead to errors when calculating wave speed and separating wave intensity into forward and backward components (Kolyva *et al.* 2008; Siebes *et al.* 2009).

Conclusions

This study revealed a 'smoke and mirrors' effect caused by wave reflection that obscures the true upstream and downstream contributions to early diastolic coronary waves. Experimental and computational data supported our hypothesis that the FDW_{dia}, FCW_{dia} and BDW_{dia} are all affected by wave reflection and, hence, both upstream *and* downstream forces. In particular, the dominant BDW_{dia} appears to arise from a combination of distal suction and wave reflection, with non-linear addition of the two component waves being a significant factor underlying the prominence of this wave. The FDW_{dia} and FCW_{dia} are attenuated and augmented respectively by negative

reflection of the BDW_{dia} at the coronary ostium. These findings have significant implications for the prevailing interpretation of the coronary wave intensity profile. We also proposed techniques for recovering the waves arising from non-reflection-related upstream forces (for forward waves) and downstream forces (for backward waves). While the precise contribution of wave reflection and active mechanisms in humans under various conditions must be established in future studies, the principles and techniques described in this study are likely to have an important impact on the interpretation of coronary wave intensity profiles in health and disease.

Appendix 1

Model parameters

Cardiovascular model. Parameters for the closed-loop cardiovascular model were taken from Mynard *et al.* (2012) and adjusted to represent an older adult arterial system with target haemodynamic values described in the Methods. Parameters governing the heart chambers, valves, 1D segments and vascular beds shown in Fig. 4 are given in A1–A4.

One-dimensional conduit coronary arteries. The geometry of the right-dominant 1D coronary conduit arterial model (i.e. reference cross-sectional area, length and connectivity of all 1D segments) was identical to that in Mynard & Smolich (2016*a*) and is therefore not reproduced here. The only difference was that, compared with the model in Mynard & Smolich (2016*a*), the wave speed of all segments was increased by 250% compared with those representing a healthy young circulation, resulting in a proximal LAD wave speed of 20.8 m s^{-1}, similar to reported values in older adult patients (Davies *et al.* 2006*a*; Rolandi *et al.* 2012).

Coronary microcirculation model. Terminal 1D segments perfuse parts of the LV free wall (LVfw), right ventricular free wall (RVfw) and septum (Sep). As in previous work (Mynard *et al.* 2014; Mynard & Smolich, 2016*a*), total microcirculatory resistance (i.e. $R_1 + R_m + R_2$ in Fig. 4*C*) was determined iteratively to achieve a target mean flow (2.54%, 0.66% and 1.35% of cardiac output, for the LVfw, RVfw and septum respectively). This flow was distributed amongst instances of the 0D model in proportion to their myocardial weights, which in turn were distributed according to the inverse cube of penetrating artery radii (i.e. Murray's law). Total weights for the adult human LVfw, RVfw and septum of 104, 46 and 54 g respectively were taken from Lorenz *et al.* (1999). Subendocardial-to-subepicardial flow ratios (1.24 and 1.18 for LVfw and RVfw) and left-to-right septal flow ratios (1.37) were taken from Fisher *et al.* (1982). We

Table A1. Model parameters for heart chambers

	LV	RV	LA	RA
E_{max} (mmHg mL^{-1})	2.2	0.35	0.13	0.09
E_{min} (mmHg mL^{-1})	0.07	0.035	0.09	0.045
V_0 (mL)	10	60	3	7
$V_{t=0}$ (mL)	150	155	80	60
K_S (10^{-3} s mL^{-1})	1.00	1.00	0.25	0.50
τ_1 (s)	0.215	0.215	0.042	0.042
τ_2 (s)	0.362	0.362	0.138	0.138
m_1 (–)	1.32	1.32	1.99	1.99
m_2 (–)	21.9	21.9	11.2	11.2
κ (–)	6	6	2	2
μ_{AV} (g cm^{-7} s^{-1})	0	0	0.033	0.05
t_{onset} (s)	0	0	0.65	0.65

E_{max}, maximum free wall elastance; E_{min}, minimum free wall elastance; V_0, pressure-axis intercept of the pressure–volume relation; $V_{t=0}$, initial chamber volume; K_S, source resistance coefficient; τ_1/τ_2, contraction/relaxation time constants; m_1/m_2, contraction/relaxation rate constants; κ, septal elastance constant (ventricular interaction via the septum); μ_{AV}, atrioventricular plane piston constant (atrioventricular interaction); t_{onset}, onset time of contraction. Note: no pericardial constraint was applied. See Mynard and Smolich (2015) for an explanation of these parameters.

Table A2. Model parameters for heart valves

	Av	Pv	Mv	Tv	Vv
$A_{eff,max}$ (cm^2)	4.9	5.7	5.1	6	6
$A_{eff,min}$ (cm^2)	0.0	0.0	0.0	0.0	0.0
l_{eff} (cm)	1.5	1.5	2	2	1.5
K_{vo} (cm^2 s^2 g^{-1})	0.02	0.02	0.02	0.03	0.03
K_{vc} (cm^2 s^2 g^{-1})	0.02	0.02	0.04	0.04	0.03

$A_{eff,max}$, maximum effective valve area (when fully open); $A_{eff,max}$, minimum effective valve area (when closed); l_{eff}, effective length; K_{vo}, valve opening rate coefficient; K_{vc}, valve closure rate coefficient. Valve abbreviations: Av, aortic valve; Pv, pulmonary valve; Mv, mitral valve; Tv, tricuspid valve; Vv, venous valve. See Mynard *et al.* (2012) and Mynard and Smolich (2015) for an explanation of these parameters.

Table A3. Model parameters for one-dimensional segments of the cardiovascular model (see Fig. 4B)

	L (cm)	A_0 (cm^2)	c_0 (cm/s)	P_0 (mmHg)
LVot	1	7.2	900	90
AoRt	1	7.2	900	90
SA	40	7.2 → 5.0	900 → 1286	90
SV1	10	6	150	4.5
SV2	5	6	150	4.5
RVot	1	7.1	250	14
PA	5	7.1 → 10.6	250	14
PV	5	10	150	8.5

L is segment length. A_0, c_0 and P_0 are reference cross-sectional area, wave speed and pressure. Abbreviations: LVot, left ventricular outflow tract; AoRt, aortic root proximal to the coronary ostia; SA, systemic artery; SV, systemic vein (two segments separated by a venous valve); RVot, right ventricular outflow tract; PA, pulmonary artery; PV, pulmonary vein. Arrows indicate linear tapering from proximal to distal values.

assumed $R_1 = 1.2R_m$ and $R_2 = 0.5R_m$ in all myocardial regions and that 75% of R_m is dependent on the volume of chamber 1 and the remainder is dependent on chamber 2 (Spaan *et al.* 2000). Compliances were set to $C_1 = 0.013$ and $C_2 = 0.254$ mL mmHg^{-1}/100 g, and reference volumes $V_{0,1} = 2.5$ and $V_{0,2} = 8.0$ mL/100 g, both with a subendocardial-to-subepicardial (or left-to-right septal) ratio of 1.14 (Weiss & Winbury, 1974; Bruinsma

Table A4. Model parameters for the vascular beds in the cardio-vascular model (see Fig. 4B)

	R_0 (mmHg.s mL^{-1})	C_{art} (mL mmHg^{-1})	C_{ven} (mL mmHg^{-1})
SVB	1.8	0.5	11
PVB	0.05	5.0	15

R_0, reference resistance; C_{art}, arterial compliance; C_{ven}, venous compliance. Vascular bed abbreviations: SVB, systemic vascular bed; PVB, pulmonary vascular bed. Note that arterial and venous characteristic impedances ($Z_{0,art}$, $Z_{0,ven}$ in Fig. 4B) were calculated from the connecting 1D segment as $\rho c_0/A_0$, where $\rho = 1.06$ g cm^{-3} is blood density (see A3).

et al. 1988). CEP was assumed to decline linearly from ventricular cavity pressure at the endocardium to pericardial pressure (assumed to be zero) at the epicardium, while SIP was assumed to be the same in each transmural layer, with a peak value equal to 20% of cavity pressure and a waveform shape identical to the ventricular chamber elastance curve (Mynard *et al.* 2014).

References

Algranati D, Kassab GS & Lanir Y (2010). Mechanisms of myocardium-coronary vessel interaction. *Am J Physiol Heart Circ Physiol* **298**, H861–873.

Arts T, Kruger RT, van Gerven W, Lambregts JA & Reneman RS (1979). Propagation velocity and reflection of pressure waves in the canine coronary artery. *Am J Physiol Heart Circ Physiol* **237**, H469–474.

Bednarik JA & May CN (1995). Evaluation of a transit-time system for the chronic measurement of blood flow in conscious sheep. *J Appl Physiol* **78**, 524–530.

Bessems D, Rutten M & Van de Vosse FN (2007). A wave propagation model of blood flow in large vessels using an approximate velocity profile function. *J Fluid Mech* **580**, 145–168.

Brosh D, Higano ST, Slepian MJ, Miller HI, Kern MJ, Lennon RJ, Holmes DR Jr & Lerman A (2002). Pulse transmission coefficient: a novel nonhyperemic parameter for assessing the physiological significance of coronary artery stenoses. *J Am Coll Cardiol* **39**, 1012–1019.

Broyd CJ, Nijjer S, Sen S, Petraco R, Jones S, Al-Lamee R, Foin N, Al-Bustami M, Sethi A, Kaprielian R, Ramrakha P, Khan M, Malik I, Francis D, Parker KH, Hughes AD, Mikhail G, Mayet J & Davies JE (2016). Estimation of coronary wave intensity analysis using non-invasive techniques and its application to exercise physiology. *Am J Physiol Heart Circ Physiol* **210**, H619–627.

Bruinsma P, Arts T, Dankelman J & Spaan JAE (1988). Model of the coronary circulation based on pressure dependence of coronary resistance and compliance. *Basic Res Cardiol* **83**, 510–524.

Claridge S, Chen Z, Jackson T, De Silva K, Behar J, Sohal M, Webb J, Hyde E, Lumley M, Asrress K, Williams R, Bostock J, Ali M, Gill J, O'Neill M, Razavi R, Niederer S, Perera D & Rinaldi CA (2015). Effects of epicardial and endocardial cardiac resynchronization therapy on coronary flow: insights from wave intensity analysis. *J Am Heart Assoc* **4**, e002626.

Covert RF, Drummond WH, Gimotty PA & Carter RL (1989). Chloralose alters both basal hemodynamics and cardiovascular responses to alveolar hypoxia in chronically instrumented, spontaneously breathing lambs. *Pediatr Res* **25**, 389–395.

Cox RH (1972). Influence of chloralose anesthesia on cardiovascular function in trained dogs. *Am J Physiol* **223**, 660–667.

Davies JE, Sen S, Broyd C, Hadjiloizou N, Baksi J, Francis DP, Foale RA, Parker KH, Hughes AD, Chukwuemeka A, Casula R, Malik IS, Mikhail GW & Mayet J (2011). Arterial pulse wave dynamics after percutaneous aortic valve replacement. *Circulation* **124**, 1565–1572.

Davies JE, Whinnett ZI, Francis DP, Manisty CH, Aguado-Sierra J, Willson K, Foale RA, Malik IS, Hughes AD, Parker KH & Mayet J (2006a). Evidence of a dominant backward-propagating "suction" wave responsible for diastolic coronary filling in humans, attenuated in left ventricular hypertrophy. *Circulation* **113**, 1768–1778.

Davies JE, Whinnett ZI, Francis DP, Willson K, Foale RA, Malik IS, Hughes AD, Parker KH & Mayet J (2006b). Use of simultaneous pressure and velocity measurements to estimate arterial wave speed at a single site in humans. *Am J Physiol Heart Circ Physiol* **290**, 878–885.

De Silva K, Foster P, Guilcher A, Bandara A, Jogiya R, Lockie T, Chowiencyzk P, Nagel E, Marber M, Redwood S, Plein S & Perera D (2013). Coronary wave energy: a novel predictor of functional recovery after myocardial infarction. *Circ Cardiovasc Interv* **6**, 166–175.

De Silva K, Lumley M, Kailey B, Alastruey J, Guilcher A, Asrress KN, Plein S, Marber M, Redwood S & Perera D (2014). Coronary and microvascular physiology during intra-aortic balloon counterpulsation. *JACC Cardiovasc Interv* **7**, 631–640.

Dodge JT Jr, Brown BG, Bolson EL & Dodge HT (1992). Lumen diameter of normal human coronary arteries. Influence of age, sex, anatomic variation, and left ventricular hypertrophy or dilation. *Circulation* **86**, 232–246.

Fisher DJ, Heymann MA & Rudolph AM (1982). Regional myocardial blood flow and oxygen delivery in fetal, newborn, and adult sheep. *Am J Physiol Heart Circ Physiol* **243**, H729–731.

Guiot C, Pianta G, Cancelli C & Pedley TJ (1990). Prediction of coronary blood flow with a numerical model based on collapsible tube dynamics. *Am J Physiol Heart Circ Physiol* **258**, H1606–1614.

Hadjiloizou N, Davies JE, Malik IS, Aguado-Sierra J, Willson K, Foale RA, Parker KH, Hughes AD, Francis DP & Mayet J (2008). Differences in cardiac microcirculatory wave patterns between the proximal left mainstem and proximal right coronary artery. *Am J Physiol Heart Circ Physiol* **295**, H1198–1205.

Heineman FW & Grayson J (1985). Transmural distribution of intramyocardial pressure measured by micropipette technique. *Am J Physiol Heart Circ Physiol* **249**, H1216–1223.

Hollander EH, Wang JJ, Dobson GM, Parker KH & Tyberg JV (2001). Negative wave reflections in pulmonary arteries. *Am J Physiol Heart Circ Physiol* **281**, H895–902.

Hughes AD, Parker KH & Davies JE (2008). Waves in arteries: a review of wave intensity analysis in the systemic and coronary circulations. *Artery Res* **2**, 51–59.

Jones CJ, Sugawara M, Kondoh Y, Uchida K & Parker KH (2002). Compression and expansion wavefront travel in canine ascending aortic flow: wave intensity analysis. *Heart Vessels* **16**, 91–98.

Kemp BK, Smolich JJ, Ritchie BC & Cocks TM (1995). Endothelium-dependent relaxations in sheep pulmonary arteries and veins: resistance to block by N^G-nitro-L-arginine in pulmonary hypertension. *Br J Pharmacol* **116**, 2457–2467.

Khir AW, O'Brien A, Gibbs JS & Parker KH (2001). Determination of wave speed and wave separation in the arteries. *J Biomech* **34**, 1145–1155.

Khir AW & Parker KH (2005). Wave intensity in the ascending aorta: effects of arterial occlusion. *J Biomech* **38**, 647–655.

Kolyva C, Spaan JAE, Piek JJ & Siebes M (2008). Windkesselness of coronary arteries hampers assessment of human coronary wave speed by single-point technique. *Am J Physiol Heart Circ Physiol* **295**, H482–490.

Kyriacou A, Whinnett ZI, Sen S, Pabari PA, Wright I, Cornelussen R, Lefroy D, Davies DW, Peters NS, Kanagaratnam P, Mayet J, Hughes AD, Francis DP & Davies JE (2012). Improvement in coronary blood flow velocity with acute biventricular pacing is predominantly due to an increase in a diastolic backward-travelling decompression (suction) wave. *Circulation* **126**, 1334–1344.

Ladwiniec A, White PA, Nijjer SS, O'Sullivan M, West NEJ, Davies JE & Hoole SP (2016). Diastolic backward-traveling decompression (suction) wave correlates with simultaneously acquired indices of diastolic function and is reduced in left ventricular stunning. *Circ Cardiovasc Interv* **9**, e003779.

Lee J, Nordsletten D, Cookson A, Rivolo S & Smith N (2016). In silico coronary wave intensity analysis: application of an integrated one-dimensional and poromechanical model of cardiac perfusion. *Biomech Model Mechanobiol* **15**, 1535–1555.

Liu Y, Zhang W & Kassab GS (2008). Effects of myocardial constraint on the passive mechanical behaviors of the coronary vessel wall. *Am J Physiol Heart Circ Physiol* **294**, H514–523.

Lockie TPE, Rolandi MC, Guilcher A, Perera D, De Silva K, Williams R, Asrress KN, Patel K, Plein S, Chowienczyk P, Siebes M, Redwood SR & Marber MS (2012). Synergistic adaptations to exercise in the systemic and coronary circulations that underlie the warm-up angina phenomenon. *Circulation* **126**, 2565–2574.

Lorenz CH, Walker ES, Morgan VL, Klein SS & Graham TP (1999). Normal human right and left ventricular mass, systolic function, and gender differences by cine magnetic resonance imaging. *J Cardiovasc Magn Reson* **1**, 7–21.

Lu P-J, Yang C-FJ, Wu M-Y, Hung C-H, Chan M-Y & Hsu T-C (2011). Wave energy patterns of counterpulsation: a novel approach with wave intensity analysis. *J Thorac Cardiovasc Surg* **142**, 1205–1213.

Lu P-J, Yang C-FJ, Wu M-Y, Hung C-H, Chan M-Y & Hsu T-C (2012). Wave intensity analysis of para-aortic counterpulsation. *Am J Physiol Heart Circ Physiol* **302**, H1481–1491.

Mirsky I (1984). Assessment of diastolic function: suggested methods and future considerations. *Circulation* **69**, 836–841.

Mitchell GF, Lacourciere Y, Ouellet J-P, Izzo JL Jr, Neutel J, Kerwin LJ, Block AJ & Pfeffer MA (2003). Determinants of elevated pulse pressure in middle-aged and older subjects with uncomplicated systolic hypertension: the role of proximal aortic diameter and the aortic pressure-flow relationship. *Circulation* **108**, 1592–1598.

Mynard JP, Davidson MR, Penny DJ & Smolich JJ (2012). A simple, versatile valve model for use in lumped parameter and one-dimensional cardiovascular models. *Int J Num Meth Biomed Eng* **28**, 626–641.

Mynard JP, Kowalski R, Cheung MMH & Smolich JJ (2017). Beyond the aorta: partial transmission of reflected waves from aortic coarctation into supra-aortic branches modulates cerebral hemodynamics and left ventricular load. *Biomech Model Mechanobiol* **16**, 635–650.

Mynard JP & Nithiarasu P (2008). A 1D arterial blood flow model incorporating ventricular pressure, aortic valve and regional coronary flow using the locally conservative Galerkin (LCG) method. *Comm Num Meth Eng* **24**, 367–417.

Mynard JP, Penny DJ & Smolich JJ (2008). Accurate automatic detection of end-diastole from left ventricular pressure using peak curvature. *IEEE Trans Biomed Eng* **55**, 2651–2657.

Mynard JP, Penny DJ & Smolich JJ (2014). Scalability and in vivo validation of a multiscale numerical model of the left coronary circulation. *Am J Physiol Heart Circ Physiol* **306**, H517–528.

Mynard JP & Smolich JJ (2015). One-dimensional haemodynamic modeling and wave dynamics in the entire adult circulation. *Ann Biomed Eng* **43**, 1443–1460.

Mynard JP & Smolich JJ (2016a). Influence of anatomical dominance and hypertension on coronary conduit arterial and microcirculatory flow patterns: a multi-scale modeling study. *Am J Physiol Heart Circ Physiol* **311**, H11–23.

Mynard JP & Smolich JJ (2016b). Novel wave power analysis linking pressure-flow waves, wave potential and the forward and backward components of hydraulic power. *Am J Physiol Heart Circ Physiol* **310**, H1026–1038.

Narayan O, Leung MCH, Wong DTL, Meredith IT & Cameron JD (2015). Percutaneous coronary intervention enhances accelerative wave intensity in coronary arteries. *PLoS ONE* **10**, e0142998.

Parker KH & Jones CJ (1990). Forward and backward running waves in the arteries: analysis using the method of characteristics. *J Biomech Eng* **112**, 322–326.

Parker KH, Jones CJ, Dawson JR & Gibson DG (1988). What stops the flow of blood from the heart? *Heart Vessels* **4**, 241–245.

Parkes DG, Vaughan J, Rivier J, Vale W & May CN (1997). Cardiac inotropic actions of urocortin in conscious sheep. *Am J Physiol Heart Circ Physiol* **272**, H2115–2122.

Penny DJ, Mynard JP & Smolich JJ (2008). Aortic wave intensity analysis of ventricular-vascular interaction during incremental dobutamine infusion in adult sheep. *Am J Physiol Heart Circ Physiol* **294**, H481–489.

Penny DJ & Smolich JJ (2002). Divergent effects of NO synthase inhibition on systemic and myocardial O_2 delivery and consumption during dobutamine infusion in sheep. *Pflügers Arch Eur J Physiol* **443**, 601–608.

Pijls NHJ, Kern MJ, Yock PG & De Bruyne B (2000). Practice and potential pitfalls of coronary pressure measurement. *Catheter Cardiovasc Interv* **49**, 1–16.

Rabbany SY, Kresh JY & Noordergraaf A (1989). Intramyocardial pressure: interaction of myocardial fluid pressure and fiber stress. *Am J Physiol Heart Circ Physiol* **257**, H357–364.

Ramaswamy SD, Vigmostad SC, Wahle A, Lai YG, Olszewski ME, Braddy KC, Brennan TMH, Rossen JD, Sonka M & Chandran KB (2004). Fluid dynamic analysis in a human left anterior descending coronary artery with arterial motion. *Ann Biomed Eng* **32**, 1628–1641.

Ramsey MW & Sugawara M (1997). Arterial wave intensity and ventriculoarterial interaction. *Heart Vessels* (Suppl 12), 128–134.

Raphael CE, Cooper R, Parker KH, Collinson J, Vassiliou V, Pennell DJ, de Silva R, Hsu LY, Greve AM, Nijjer S, Broyd C, Ali A, Keegan J, Francis DP, Davies JE, Hughes AD, Arai A, Frenneaux M, Stables RH, Di Mario C & Prasad SK (2016). Mechanisms of myocardial ischemia in hypertrophic cardiomyopathy: insights from wave intensity analysis and magnetic resonance. *J Am Coll Cardiol* **68**, 1651–1660.

Rivolo S, Hadjilucas L, Sinclair M, van Horssen P, van den Wijngaard J, Wesolowski R, Chiribiri A, Siebes M, Smith NP & Lee J (2016). Impact of coronary bifurcation morphology on wave propagation. *Am J Physiol Heart Circ Physiol* **311**, H855–870.

Rolandi MC, Nolte F, van de Hoef TP, Remmelink M, Baan J, Piek JJ, Spaan JAE & Siebes M (2012). Coronary wave intensity during the valsalva manoeuvre in humans reflects altered intramural vessel compression responsible for extravascular resistance. *J Physiol* **590**, 4623–4635.

Rumberger JA Jr, Nerem RM & Muir WW III (1979). Coronary artery pressure development and wave transmission characteristics in the horse. *Cardiovasc Res* **13**, 413–419.

Siebes M, Kolyva C, Verhoeff B-J, Piek J & Spaan J (2009). Potential and limitations of wave intensity analysis in coronary arteries. *Med Biol Eng Comput* **47**, 233–239.

Sinclair MD, Lee J, Cookson AN, Rivolo S, Hyde ER & Smith NP (2015). Measurement and modeling of coronary blood flow. *Wiley Interdiscip Rev Syst Biol Med* **7**, 335–356.

Smolich JJ & Mynard JP (2016). A step towards clinically applicable non-invasive coronary wave intensity analysis. *Am J Physiol Heart Circ Physiol* **310**, H525–527.

Spaan JA (1985). Coronary diastolic pressure-flow relation and zero flow pressure explained on the basis of intramyocardial compliance. *Circ Res* **56**, 293–309.

Spaan JAE, Cornelissen AJM, Chan C, Dankelman J & Yin FCP (2000). Dynamics of flow, resistance, and intramural vascular volume in canine coronary circulation. *Am J Physiol Heart Circ Physiol* **278**, H383–403.

Stein PD, Sabbah HN & Marzilli M (1985). Intramyocardial pressure and coronary extravascular resistance. *J Biomech Eng* **107**, 46–50.

Sun YH, Anderson TJ, Parker KH & Tyberg JV (2000). Wave-intensity analysis: a new approach to coronary hemodynamics. *J Appl Physiol* **89**, 1636–1644.

Sun YH, Anderson TJ, Parker KH & Tyberg JV (2004). Effects of left ventricular contractility and coronary vascular resistance on coronary dynamics. *Am J Physiol Heart Circ Physiol* **286**, H1590–1595.

Weiss HR & Winbury MM (1974). Nitroglycerin and chromonar on small-vessel blood content of the ventricular walls. *Am J Physiol* **226**, 838–843.

Additional information

Conflicts of interest

None.

Author contributions

JPM: conception and design, computational studies, data analysis, preparation of figures and manuscript; DJP and JJS: design and conduct of laboratory experiments. All authors edited and revised the manuscript, approved the final version and agree to be accountable for all aspects of the work. All persons designated as authors qualify for authorship, and all those who qualify for authorship are listed.

Funding

Acknowledgements

Translational perspective

Wave intensity analysis is an emerging technique that is being used to unravel the upstream (aortic) and downstream (intramyocardial) forces that determine coronary blood flow. A dominant backward decompression wave (BDW_{dia}) accompanies the early-diastolic surge in coronary flow and, based on a number of published studies, has been shown to have potential clinical value. To date, it has been widely held that the BDW_{dia} is generated in the coronary microvasculature via a suction effect caused by myocardial relaxation. Our study provides evidence that another mechanism contributes to the BDW_{dia}, namely passive wave reflection of a forward wave entering the coronary arteries from the aorta. We also show that summation of the wave reflection and myocardial relaxation forces is non-linear, i.e. the resultant combined wave is substantially larger than the simple sum of waves from each mechanism acting in isolation. This finding may impact on the interpretation of clinical studies assessing BDW_{dia} magnitude under healthy or disease conditions and how it changes with intervention. With an additional measurement of ascending aortic wave intensity, the separate contributions of wave reflection and myocardial relaxation to BDW_{dia} may be estimated, thus providing more detailed and accurate insights into the upstream and downstream forces that determine coronary flow.